inorganics

MDPI

Article

Gold(III) Complexes with 18-Crown-6, 1-Aza-18-Crown-6, and Cryptands 22 and 222: Stability and Structure

Daniil N. Yarullin, Olga I. Logacheva, Viktor V. Aleksandriiskii, Maksim N. Zavalishin and George A. Gamov *

Department of General Chemical Technology, Ivanovo State University of Chemistry and Technology, Sheremetevskii Ave. 7, 153000 Ivanovo, Russia; yarullin_dn@isuct.ru (D.N.Y.); o.logachiova@yandex.ru (O.I.L.); nmr@isuct.ru (V.V.A.); zavalishin00@gmail.com (M.N.Z.)

* Correspondence: ggamov@isuct.ru; Tel.: +7-91-5821-8562

Abstract

The growing demand for gold in various high-technology applications necessitates the development of efficient and selective methods for its recovery and analysis, which can be achieved using such macrocyclic ligands as crown esters and their aza-substituted derivatives. The present paper reports on the equilibrium constants for the formation of gold(III) complexes with 18-crown-6, 1-aza-18-crown-6, 1,10-diaza-18-crown-6, and the cryptand 4,7,13,16,21,24-hexaoxa-1,10-diazabicyclo[8.8.8]hexacosane (Kryptofix 222) in aqueous solution at T = 298.2 K, p = 0.1 MPa, $I \rightarrow 0$. The equilibrium constants (log β) for the substitution of chloride ions by macrocycles were determined to be 4.52 ± 0.04, 9.15 ± 0.03, 9.08 ± 0.07, and 11.51 ± 0.08, respectively. Equilibrium constants for protonated and polyligand species are also provided. The complexation mechanism was elucidated using a combination of spectroscopic techniques. UV-Vis and IR spectroscopy confirm the substitution of chloride ligands by the nitrogen donor atoms of the aza-macrocycles within the tetrachloroaurate(III) ion. Furthermore, ^{1}H NMR analysis reveals that the diaza-substituted ligands can form both inclusion complexes, where the gold cation is encapsulated within the macrocyclic cavity, and exclusion complexes. These findings provide a quantitative foundation for the design of novel macrocycle-based extractants and sensors for gold(III).

Keywords: gold(III); crown ester; cryptand; complexation; stability constant; protonation

1. Introduction

Crown ethers are cyclic molecules characterized by a repeating unit of the form −R−O−R−R−O−R−. Their defining structural feature is a central cavity, which allows them to act as essentially two-dimensional complexing agents. A key advantage of this architecture is its inherent size selectivity: the cavity dimensions can be matched to the ionic radius of a target cation. For instance, the 18-crown-6 ether exhibits an optimal fit for K^+, while 15-crown-5 is better suited for the smaller Na^+ [1,2].

The substitution of one or more oxygen atoms in the polyether chain with nitrogen (aza-substitution) provides two significant enhancements. First, it can increase the ligand's affinity for various cations. Second, it enables the introduction of a third bridging chain, transforming the planar cycle into a three-dimensional cage structure [1,2].

The practical value of crown ethers is largely determined by their ability to form stable complexes with metal ions and certain other species, such as protonated primary amines [3].

Check for updates

Academic Editors: Wanhe Wang, Jing Wang and Xiao Yao

Received: 11 March 2026
Revised: 27 March 2026
Accepted: 27 March 2026
Published: 29 March 2026

Copyright: © 2026 by the authors. Licensee MDPI, Basel, Switzerland. This article is an open access article distributed under the terms and conditions of the Creative Commons Attribution (CC BY) license.

In pharmaceutical applications, for example, they are investigated as solubilizers to improve the bioavailability of poorly soluble drugs and to facilitate their permeation across mucosal membranes [4,5]. However, while crown ethers demonstrate some antimicrobial potential [6,7], their inherent toxicity, stemming from their ability to bind biologically relevant alkali metal cations, poses a significant challenge to their implementation in medical practice [8,9].

Gold holds immense importance in human activities (especially in fabricating chip and electronic devices) due to its unique combination of physical and chemical properties, *viz*. corrosion resistance, high electrical and thermal conductivity, and malleability. With the exponential growth of electronic waste, recovering gold from secondary sources (so-called "urban mining" [10]) has become an urgent environmental and economic priority, necessitating the development of highly selective and efficient extraction agents. The high affinity of crown ethers for various ions makes them attractive candidates for the extraction, separation [11–14], and identification [15,16] of valuable metals, including gold.

According to the hardiness/softness of acids/bases principle [17], the substitution of hard oxygen donors with softer nitrogen atoms is expected to significantly enhance the binding affinity for gold(III), a classic soft acid, thereby providing a rational basis for ligand design. We hypothesized that progressive aza-substitution and the transition from a planar macrocycle to a three-dimensional cryptand would systematically increase the stability of the resulting gold(III) complexes. That is why in this study, we investigate how aza-substitution and the introduction of an additional side chain influence the stability of gold(III) complexes with a series of macrocyclic ligands. The ligands under study are 18-crown-6 (18C6) and three of its derivatives: 1-aza-18-crown-6 (1N18C6), 1,10-diaza-18-crown-6 (hereafter referred to as [2.2]), and the cryptand 4,7,13,16,21,24-hexaoxa-1,10-diazabicyclo[8.8.8]hexacosane (hereafter referred to as [2.2.2]). Their structures are presented in Figure 1.

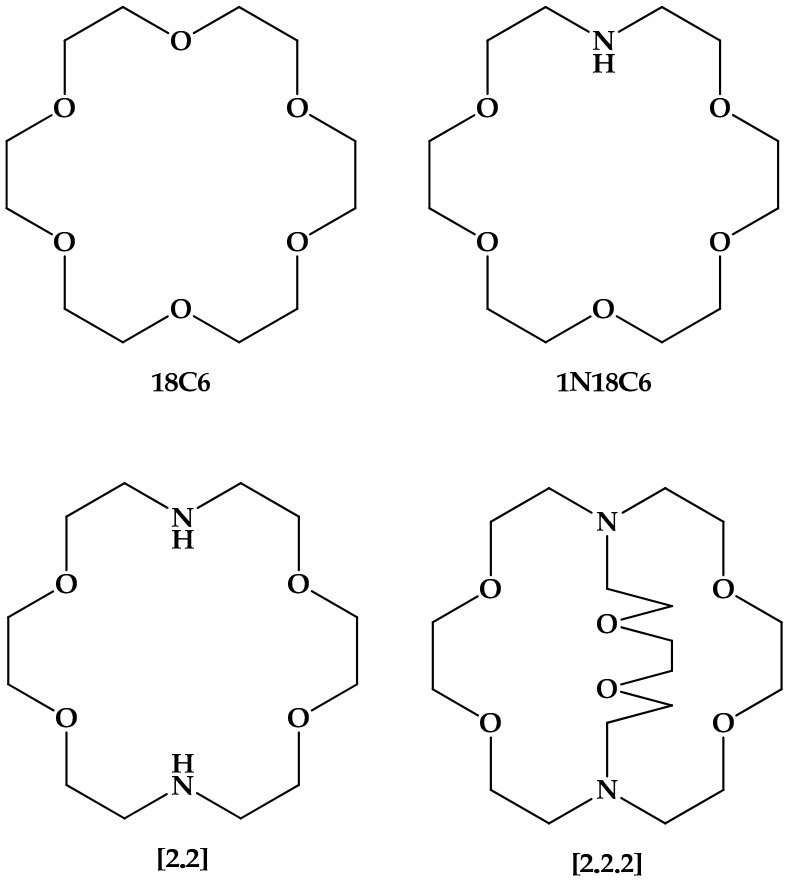


Figure 1. Macrocyclic ligands under study forming complexes with gold(III).

Although several studies have explored gold(III) complexes with N-donor ligands, systematic data on their stability remain limited [18]. To date, chloride substitution at tetrachloroaurate(III) has been investigated for pyridine [19], 2,2′-dipyridine, 1,10-phenantroline [20], ethylenediamine [21], propylenediamine [22,23], and diethylenetriamine [21]. Notably, diaza-substituted crown ethers can be viewed as cyclized analogues of linear diamines, making them particularly suitable for assessing the effect of macrocyclic constraint on complex stability.

The stability constants for the formation of gold(III) complexes with these ligands in aqueous solution were determined potentiometrically and spectrophotometrically at T = 298 K, p = 0.1 MPa, and $I \rightarrow 0$. Furthermore, special attention is given to elucidating the structure of the resulting complexes, which was investigated using a combination of ^{1}H NMR, IR, and UV-Vis spectroscopy.

2. Results and Discussion

2.1. Basicity of Ligands

Prior to investigating complex formation, it was necessary to refine the protonation constants (pK_a) of the ligands under study because of two reasons. First, gold(III) is taken in form of tetrachloroauric(III) acid, and protonation of ligand is inevitable upon addition of $H[AuCl_4]$ to the solutions of aza-substituted crown esters. Neutralization of acid would result in intensification of tetrachloroaurate(III) hydrolysis, which would interfere with the complexation with macrocycles. Second, the performance of potentiometric setup and software used for processing the experimental data should be checked on simple experiments before the more complicated ones.

The determined values are presented in Table 1 (See Section 3.4 for the details of constant calculations). Representative examples of the experimental EMF data, along with the corresponding calculated curves, are provided in Figure S1.

Table 1. pK_a values of 1N18C6, [2.2] and [2.2.2] ligands determined in aqueous solution at T = 298.2 K, p = 0.1 MPa and $I \rightarrow 0$.

Macrocyclic Ligand	1N18C6	[2.2]	[2.2.2]
pK_{a1}	8.26 ± 0.13 (9.41 [24,25]; 8.30 [26])	9.08 ± 0.07 (8.96 [27])	9.79 ± 0.31 (9.87 [28])
pK_{a2}	-	7.47 ± 0.08 (7.67 [27])	7.35 ± 0.39 (7.23 [28])

The protonation constants for the cryptands [2.2] and [2.2.2] refined in this work (Table 1) are in satisfactory agreement with the range of values reported in the literature (see comprehensive papers [27,28] collecting all the results known to the date of publication).

In contrast, the basicity of 1-aza-18-crown-6 (1N18C6) has been determined only twice, and the reported values are in significant disagreement. An early study reported a pK_a of 9.41 [24,25] which differs by more than one log unit from both a more recent determination (pK_a = 8.3 [26]) and our own experimental value (pK_a = 8.26 ± 0.13). Identifying the precise reason for this discrepancy is difficult, as the primary experimental data and a discussion of the derived values were not provided in the original reports [24,25]. However, a notable methodological difference exists: the authors of [24,25] maintained a constant ionic strength of 0.1 M using Et_4NClO_4 as a background electrolyte, whereas both our work and the study in [26] were performed under conditions where the ionic strength approached zero. Furthermore, computational predictions using Rowan Scientific [29,30] support our findings, correctly predicting the trend pK_a (1N18C6) < pK_a ([2.2]) with a

difference of approximately 0.6 log units, which is close to the difference observed in our experiments (Table 1).

Finally, 18-crown-6 (18C6) is an extremely weak base ($pK_a = -0.4$ [31]), and is effectively unable to accept protons under our experimental conditions. While this limits the use of potentiometric methods for studying equilibria involving 18C6, it also offers a significant advantage: no competing protolytic side reactions interfere with the formation of its metal complexes in solution, making it an ideal candidate for study by spectroscopic methods such as UV-Vis.

2.2. Equilibrium Constants of Chlroide Exchange by Macrocycles

The complex formation between the macrocyclic ligands and gold(III) was investigated by potentiometric titration. Representative titration curves for 1N18C6, [2.2], and [2.2.2] with a standard $H[AuCl_4]$ solution are shown in Figure 2. The equilibrium constants for the substitution of chloride ions in tetrachloroaurate(III) by the macrocyclic ligands, corresponding to the general reaction,

$$[AuCl_4]^- + L = [AuCl_{4-n}L]^{n-1} + nCl^- \quad (1)$$

are presented in Table 2 (see Section 3.4 for the details of constant calculations).

Table 2. Values of equilibrium constants of the reaction of chloride substitution by macrocyclic ligands (log $\beta_{Cl\text{-}/L}$) 1N18C6, [2.2] and [2.2.2] in tetrachloroaurate(III) determined in aqueous solution E.M.F. titration data at T = 298.2 K, p = 0.1 MPa and $I \rightarrow 0$.

Complex Stoichiometry	18C6	1N18C6	[2.2]	[2.2.2]
$[AuCl_{4-n}L]^{n-1}$	4.52 ± 0.04 *	9.15 ± 0.03	9.08 ± 0.07	11.51 ± 0.08
$[AuCl_{4-n}HL]^{n}$	-	-	12.99 ± 0.08	15.90 ± 0.10
$[AuCl_{4-n}L_2]^{n-1}$	-	16.37 ± 0.09	-	-
$[AuL_4]^{3+}$	-	-	-	33.01 ± 0.28

* The value was determined from UV-Vis spectral experiment (see Section 2.2).

The uncertainties reported in Table 2 represent the standard deviations calculated from three independent experiments.

For the ligand 1N18C6 (Figure 2a), the experimental data were best fitted using a stoichiometric model that includes the formation of two distinct complex species. The model proposes the accumulation of a 1:1 complex, $[AuCl_{4-n}L]^{n-1}$, at the end of the titration, and the formation of a 2:1 (ligand:metal) complex, $[AuCl_{4-n}L_2]^{n-1}$, in the initial stages (Figure 2a, curve labeled "calcd"). As demonstrated by the alternative fit (Figure 2a, curve labeled "calcd alt"), omitting the $[AuCl_{4-n}L_2]^{n-1}$ species from the computational model makes it impossible to satisfactorily describe several intermediate EMF values. The formation of a protonated complex, $[AuCl_{4-n}HL]^{n}$, was considered negligible in this case, as the ligand is expected to coordinate through its single nitrogen atom.

For the [2.2] ligand (Figure 2b), the titration curve could be fitted satisfactorily using a model that considers the formation of only the 1:1 complex, $[AuCl_{4-n}L]^{n-1}$, (curve labeled "calcd alt" in Figure 2b). Incorporating the formation of a protonated complex, $[AuCl_{4-n}HL]^{n}$, into the stoichiometric scheme (curve labeled "calcd" in Figure 2b) resulted in only a marginal improvement in the quality of the fit. Furthermore, several quantitative indicators suggested that this more complex model was not statistically justified. First, upon including the protonated species, the optimized stability constant for the main $[AuCl_{4-n}L]^{n-1}$ complex decreased by a negligible amount (approximately 0.02 log units).

Second, the refined value for log $\beta_{[AuCl4-nHL]n}$ was associated with a very high standard deviation (on the order of ±2 log units) when processed as a single experiment, indicating that its concentration in solution is vanishingly small and cannot be determined with confidence. Attempts to modify the experimental conditions to increase the yield of this protonated species were unsuccessful. Increasing the total H^+ concentration led primarily to protonation of the free ligand, while partial neutralization of the starting $H[AuCl_4]$ solution simply shifted the equilibrium toward the formation of the predominant $[AuCl_{4-n}L]^{n-1}$ complex.

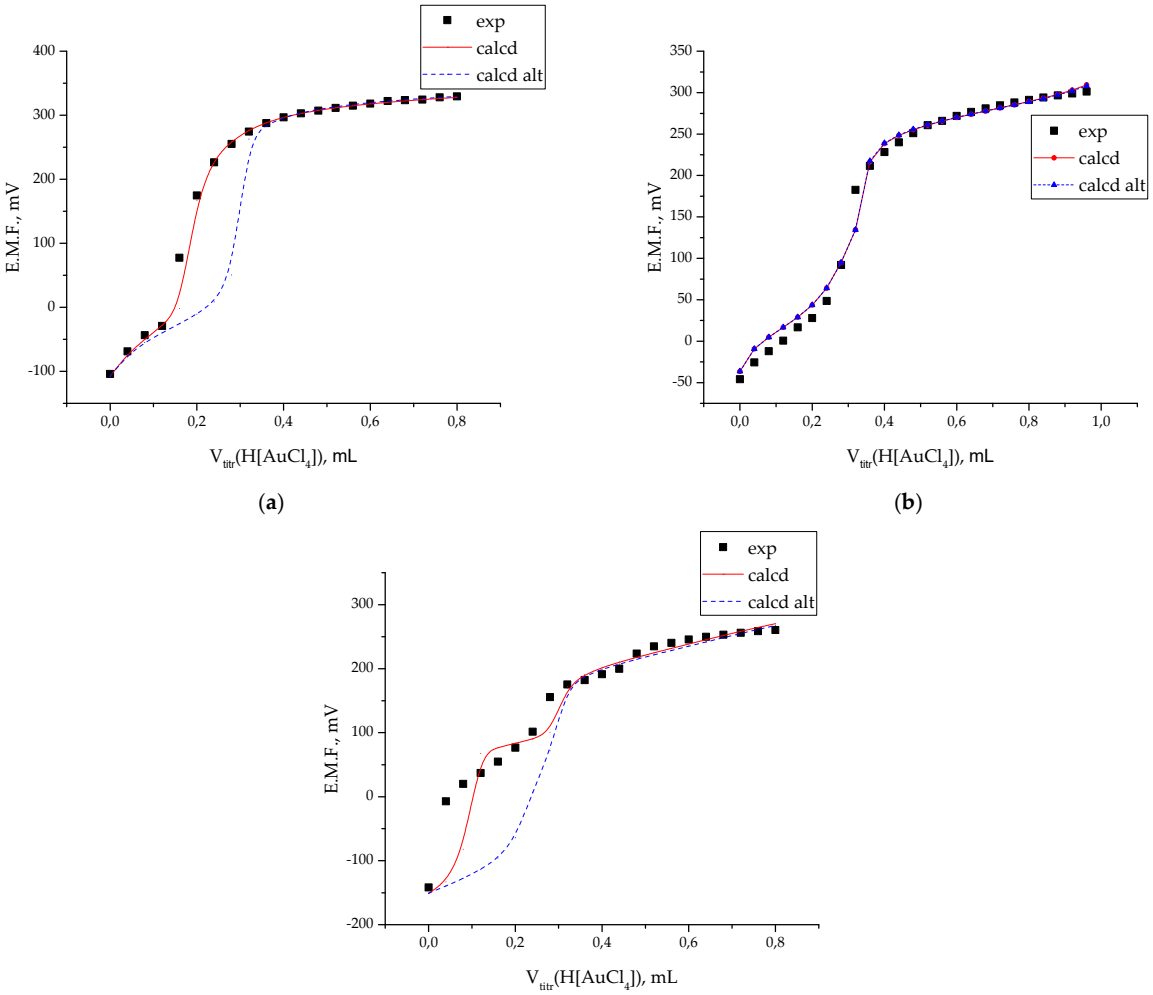


Figure 2. Examples of potentiometric titration curves of 20 mL aliquot of (**a**) 1N18C6 (0.002935 M); (**b**) [2.2] (0.002627 M); (**c**) [2.2.2] (0.002183 M) by 0.1006 M $H[AuCl_4]$ solution. Points show the experimental E.M.F. values, while lines correspond to those calculated using the optimized equilibrium constants.

The processing of the titration curves for the cryptand [2.2.2] proved to be the most complex (Figure 2c). This system exhibits a unique and reproducible feature: a sharp initial change in EMF, corresponding to a sudden increase in the free H^+ concentration of approximately 2.3 pH units. This drastic initial jump could only be satisfactorily modeled by introducing the formation of a polyligand complex with an unusual 4:1 ligand-to-metal stoichiometry, $[AuL_4]^{3+}$, into the reaction scheme (curve labeled "calcd" in Figure 2c). While the existence of such a species might seem counterintuitive, the model excluding this process fails to describe the entire first half of the potentiometric curve (curve labeled "calcd alt" in Figure 2c), leaving the initial pH drop unexplained. It is important to note that

despite its critical role in fitting the initial portion of the curve, the inclusion or exclusion of the $[AuL_4]^{3+}$ formation reaction has a negligible impact on the calculated equilibrium constants for the primary $[AuCl_{4-n}L]^{n-1}$ and protonated $[AuCl_{4-n}HL]^{n}$ complexes. Its primary effect is on the precision of these constants, influencing their calculated standard deviations rather than their refined values.

The protonation behavior of the gold(III) complexes with cryptands [2.2] and [2.2.2] is notably different from that of other metal cryptates. For example, the pK_a values of the protonated complexes $[CuH[2.2.2]]^{3+}$ [32] and $[NiH[2.2.2]]^{3+}$ [33] are only slightly lower than the dissociation constant of the free ligand, $H[2.2.2]^{+}$. In contrast, for the gold(III) complexes, the difference between the protonation constant of the $[AuCl_{4-n}L]^{n-1}$ species and that of the free ligand is remarkably large, amounting to approximately 6 log units. A tempting explanation for this discrepancy is that the ligand coordinates to gold(III) through both nitrogen atoms, analogous to the binding mode proposed for palladium(II) complexes [34]. Such bidentate coordination would render both nitrogen sites unavailable for protonation, thereby suppressing the basicity of the coordinated ligand. However, several arguments caution against the straightforward acceptance of this explanation.

First, a steric argument based on ionic radii can be made. The effective ionic radius of gold(III) (0.68 Å) is actually smaller than that of copper(II) (0.73 Å) and comparable to that of nickel(II) (0.69 Å) [35]. The complexation of nickel(II) and copper(II) does not interfere significantly with protonation [32,33] indicating that the only nitrogen is involved into complex formation. Therefore, it is unclear why gold(III) cation with the similar radius binds to both nitrogens.

Second, a thermodynamic argument based on the chelate effect points to monodentate coordination. The stepwise stability constants for gold(III) complexes with simple amines provide a useful benchmark. The equilibrium constant for the substitution of one chloride ligand by a single NH_3 molecule ($\log \beta_1$) is 6.73 [21]. In contrast, the constants for the displacement of two and three chlorides by the chelating ligands ethylenediamine and diethylenetriamine are 16.2 and 22.7 log units, respectively [21]. These values clearly demonstrate a pronounced chelate effect, where multidentate coordination results in a significant enhancement of complex stability. Crucially, the stability constants we observe for the cryptand complexes, $[AuCl_{4-n}[2.2]]^{n-1}$ and $[AuCl_{4-n}[2.2.2]]^{n-1}$, are significantly lower than would be expected for a chelated structure. In fact, they are less than twice the value for the mono-amine complex ($\log \beta < 2\log \beta_{Cl/NH3}$). The absence of any significant chelate effect is an indicator that the cryptands coordinate to the gold(III) center through only one nitrogen atom, failing to encapsulate the metal ion in a bidentate fashion. While the precise ionic radius of gold(III) can be debated [36], the thermodynamic evidence for the absence of chelation is less ambiguous.

Third, this conclusion is further supported by a direct comparison within our own data. The experimental equilibrium constants for chloride substitution by the mono-aza ligand 1N18C6 and the diaza cryptand [2.2] are remarkably similar (Table 2). If [2.2] were acting as a bidentate chelating agent, its stability constant would be expected to be substantially larger than that of 1N18C6 due to the chelate effect. The observed similarity in their constants strongly suggests that both ligands coordinate in a similar fashion, i.e., through a single nitrogen donor.

The derived equilibrium constants allow for drawing the speciation diagrams (Figure 3 shows the case of equilmolar quantities of tetrachloroaurate(III) and ligands; $C^0(Au^{3+}) = C^0(L) = 0.001$ M).

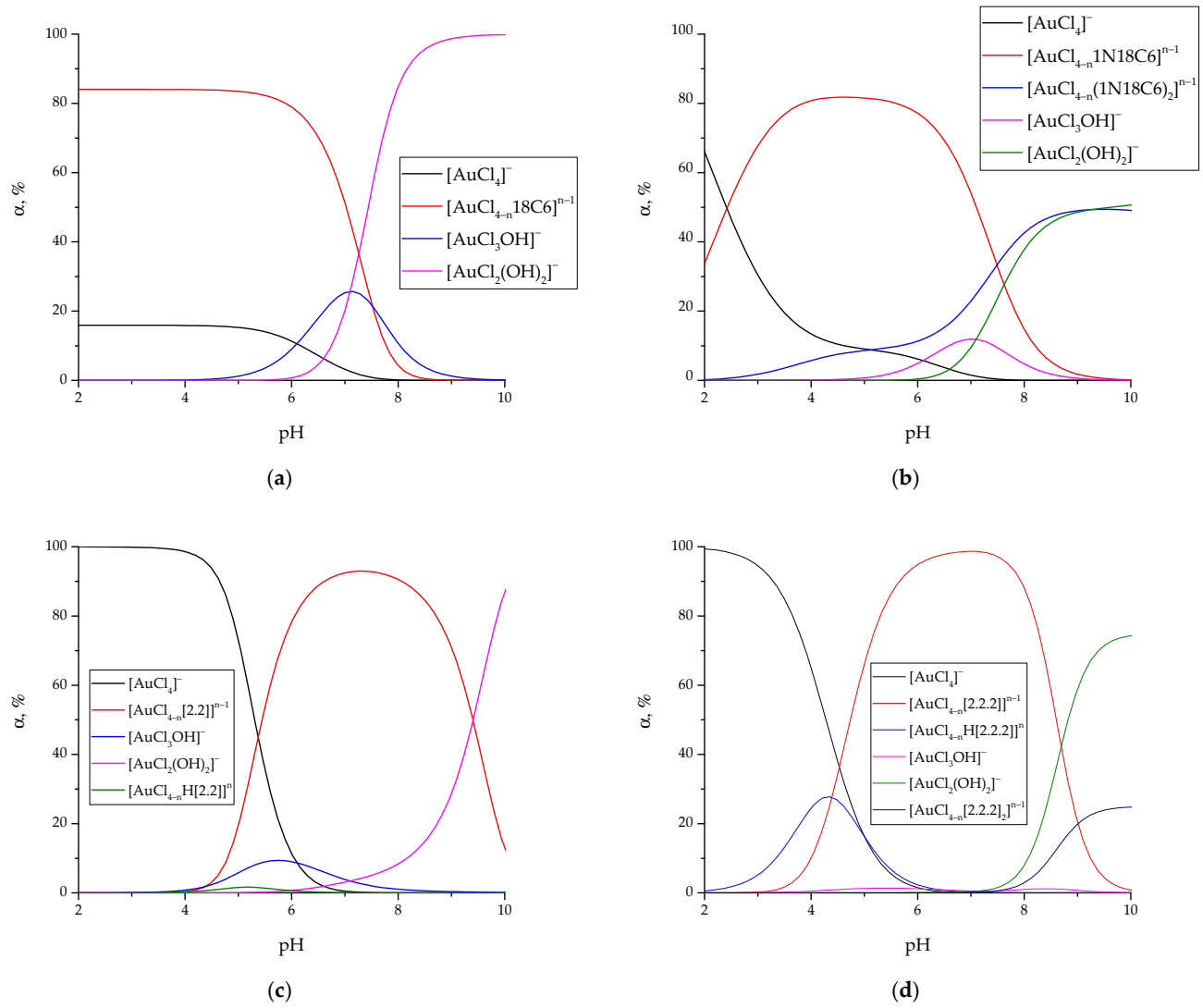


Figure 3. Speciation diagrams of gold(III) complexes formed at equimolar quantities of tetrachloroaurates(III) and macrocyclic ligands ($C^0([AuCl_4]^-) = C^0(L) = 0.001$ M): 18C6 (**a**); 1N18C6 (**b**); [2.2] (**c**); [2.2.2] (**d**).

The data in Figure 3 indicate that increasing ligand basicity shifts the pH region of maximum yield of the monoligand gold(III) complex toward neutral conditions, progressing from 18C6 to 1N18C6~[2.2] and [2.2.2] (6 to 8 log units of pH). For the [2.2] ligand, the low yield of the $[AuCl_{4-n}H[2.2]]^n$ complex across the entire range of equilibrium proton concentrations is evident from Figure 3c. In contrast, the [2.2.2] ligand forms the corresponding complex in significant amounts, with the maximum yield observed at pH ~4.2 (Figure 3d). This behavior is attributed to the higher stability of the $[AuCl_{4-n}[2.2.2]]^{n-1}$ species.

It is worth noting that the potentiometric titration of [2.2] and [2.2.2] with $H[AuCl_4]$ ultimately resulted in the precipitation of solid products. The IR spectra of these precipitates, which provide further insight into the coordination modes of the ligands, will also be discussed in the following section.

2.3. Spectral Study of Gold(III) Complexes with Macrocycles

2.3.1. UV-Vis Spectral Data

UV-Vis spectroscopy was employed as an independent method to validate the equilibrium constants determined potentiometrically. This technique offers a crucial advantage: it allows the complexation to be studied under different concentration conditions and, im-

portantly, with the reagents mixed in the reverse order. While potentiometric titration involved adding $H[AuCl_4]$ to a solution of the ligand, UV-Vis titration was performed by progressively adding the ligand to a solution of $H[AuCl_4]$. Since all macrocyclic ligands are almost transparent in the UV-Vis region, the observed spectral changes arise solely from the transformations of the gold(III) coordination sphere, providing a direct probe of complex formation.

Representative examples of the UV-Vis spectral changes observed upon the addition of 18C6, 1N18C6, [2.2], and [2.2.2] to a $H[AuCl_4]$ solution are shown in Figure 4. Concentration conditions were set to allow for monitoring both short and long wavelength maxima of tetrachloroaurate(III) and forming complexes.

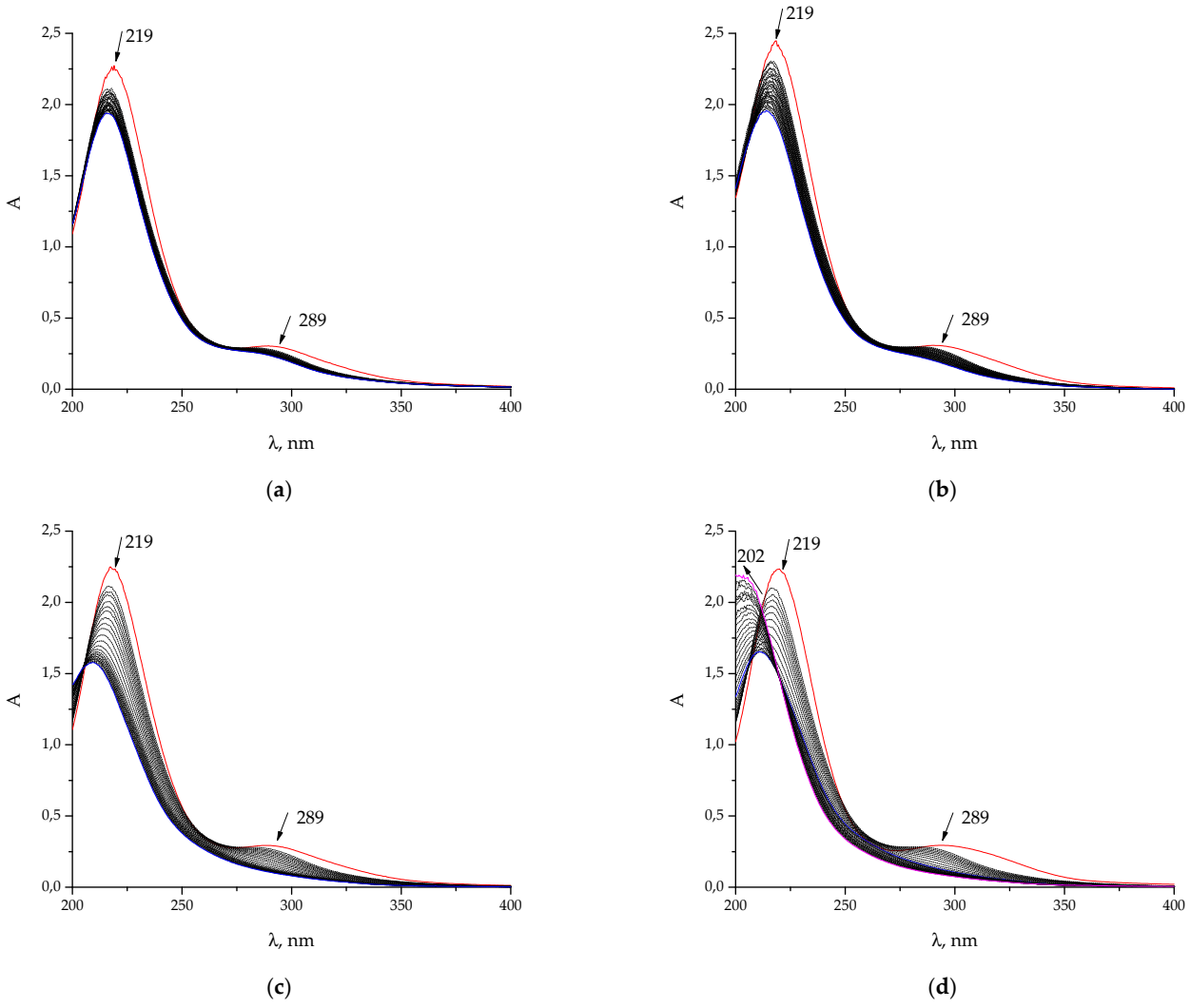


Figure 4. Changes in UV-Vis spectra of 2.52 mL of $1.229 \cdot 10^{-4}$ M $H[AuCl_4]$ solution upon titration by: (**a**) 18C6 (0.002983 M); (**b**) 1N18C6 (0.002935 M); (**c**) [2.2] (0.002627 M); (**d**) [2.2.2] (0.002183 M). 25 to 30 points were acquired; titration volume is 5 µL.

Regardless of the ligand structure, the addition of each macrocycle to a solution of $[AuCl_4]^-$ resulted in qualitatively similar spectral changes (Figure 4). The initial injection of titrant caused a pronounced hypsochromic (blue) shift of the absorption maxima, followed by a more gradual blue-shifting upon subsequent additions. This behavior is consistent with the progressive substitution of chloride ligands by the N,O-donor macrocycles (see, e.g., the changes in spectra of tetrachloroaurate(III) occurring upon chloride substitution by hydroxide ions [37–39], ammonia [40], pyridine [19], propylenediamine [23] observed

experimentally as well as the theoretical spectra obtained for mixed hydroxochloroaurates(III) [41] and chloroamminaurates(III) [42]). Compared to chloride, these ligands exert a stronger ligand field, as they lie higher in the spectrochemical series, which leads to an increase in the energy of the d-d transitions and the observed hypsochromic shift [42]. As was observed in the potentiometric experiments, the titration with cryptand [2.2.2] exhibited unique spectral features. In the initial stages, the changes mirrored those of the other ligands: the absorbance decreased, and the short-wavelength maximum shifted from 219 nm to 211 nm. However, upon a further increase in [2.2.2] concentration, an additional hypsochromic shift to approximately 202 nm occurred, accompanied by a simultaneous increase in absorbance (hyperchromic effect). This distinct spectral behavior at high ligand concentrations may be attributed to the formation of the polyligand $[Au[2.2.2]_4]^{3+}$ complex, whose existence was previously proposed to explain the unique features of the potentiometric titration curve (Section 2.2, Figure 2c).

Beyond validating the equilibrium constants derived from potentiometry, the UV-Vis titration data also enabled the calculation of the molar extinction coefficients for the individual complex species. The normalized data are presented in Figure 5.

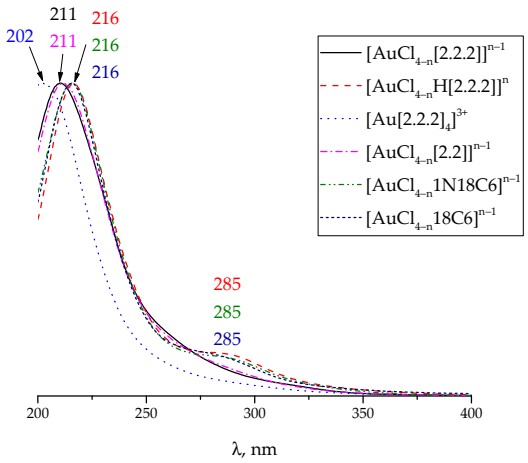


Figure 5. Normalized molar extinction coefficients of gold(III) complexes with crown esters calculated from the results of UV-Vis titration.

It was not possible to reliably calculate the molar extinction coefficients for all proposed species. Specifically, the low equilibrium concentration of the protonated complex $[AuCl_{4-n}H[2.2]]^n$ and the *bis*-ligand $[AuCl_{4-n}(1N18C6)_2]^{n-1}$ under the conditions of the UV-Vis experiment precluded their accurate determination.

Despite this limitation, a comparison of the spectra calculated from the experimental data reveals a notable pattern: the calculated spectra of the monoligand complexes can be grouped into two pairs with similar features. The spectra of the complexes with 18C6 and 1N18C6 crown esters closely resemble one another, as do the spectra of the complexes with the cryptands, [2.2] and [2.2.2]. This pairwise similarity suggests analogous coordination geometries within each group. Further insights can be gained by comparing spectra across these groups. The spectrum of the protonated complex, $[AuCl_{4-n}H[2.2.2]]^n$, is nearly identical to those of the monoligand complexes with 18C6 and 1N18C6. In contrast, the spectrum of the tetraligand species, $[Au[2.2.2]_4]^{3+}$, exhibits the most pronounced hypsochromic shift of all complexes studied.

These spectral observations can be rationalized by considering the extent of chloride substitution. A smaller hypsochromic shift correlates with a lower degree of chloride replacement in the gold(III) coordination sphere. Therefore, the cryptands [2.2] and [2.2.2] appear to form, on average, more coordination bonds with the gold(III) ion than do

the crown ethers 18C6 and 1N18C6, leading to a greater average hypsochromic shift for the cryptate complexes. This framework also allows us to interpret the behavior of the protonated and tetraligand species. The similarity of the $[AuCl_{4-n}[2.2.2]]^{n-1}$ spectrum to that of the crown ether complexes suggests that protonation may be accompanied by the re-entry of a chloride ion into the coordination sphere, effectively reducing the number of coordinated ligand donor atoms. Conversely, the extreme blue shift of the $[Au[2.2.2]_4]^{3+}$ spectrum is consistent with its formulation as a tetraligand complex, where the metal is coordinated by four nitrogen donors from four separate cryptand molecules, resulting in the highest degree of chloride substitution.

Finally, the stability constant data provide complementary support for these structural assignments. The complex with 18C6, an oxygen-donor ligand, exhibits the lowest stability constant, underscoring the higher affinity of the soft gold(III) acid for the softer nitrogen-donor ligands. The greater stability of the $[AuCl_{4-n}[2.2.2]]^{n-1}$ complex in comparison to other monoligand species might be explained by the metal ion's location within the cryptand's cavity.

2.3.2. IR Spectral Data

The IR spectra of the free cryptands [2.2] and [2.2.2], along with the spectra of the solid products that precipitated from their reaction mixtures with $H[AuCl_4]$, are shown in Figure S2 with the characteristic peaks collected in Table S1. While the spectra of the products generally retain the characteristic peaks of the free ligands (in particular, those located at 2879 and 2816 cm^{-1} referring to asymmetric and symmetric stretching of C-H bonds in methylene groups), a new vibration band appears upon complexation with gold(III). This band, located at approximately 500 cm^{-1}, is tentatively assigned to the formation of a nitrogen-gold (N–Au) coordination bond.

To extract and confirm this metal-nitrogen vibration with greater reliability, the IR spectra of both the free ligands and their gold(III) complexes were analyzed in the region from 750 to 400 cm^{-1}. The spectral envelope was deconvoluted by fitting a set of Lorentzian curves (Figure 6), following the procedure described in paper [43] and using the KEV software package (ver. 0.6.0). The optimization procedure began with the lowest possible number of fitting curves, basing the initial estimate on visible transmittance maxima. For each trial, the Lorentzian curves were shuffled multiple times to ensure reproducibility of the calculations. Only then was the next curve added until satisfactory agreement between the calculated and experimental spectra was achieved ($R^2 \rightarrow 1$).

It should be kept in mind that the presented decomposition results are possibly not free from the dangers of arbitrary curves addition, and further analysis based on high-level quantum chemical calculations might be in order.

For the free cryptand [2.2], the spectral envelope in the region of 400 to 750 cm^{-1} was best described by a set of eight Lorentzian peaks with maxima (μ) at 704.7, 658.2, 615.7, 581.1, 555.1, 521.0, 478.5, and 442.2 cm^{-1}. Upon complexation with gold(III), the spectrum of the [2.2] + H[AuCl4] precipitate required nine Lorentzian components to achieve a satisfactory fit. The fitted maxima for this complex are 694.4, 658.1, 612.1, 588.5, 556.9, 520.4, ***496.5***, 484.0, and 446.6 cm^{-1}. Notably, eight of these bands correspond closely to vibrations observed in the free ligand (with slight shifts), while the band at ***496.5*** cm^{-1} has no counterpart in the spectrum of free [2.2] and is attributed to the formation of the N–Au bond.

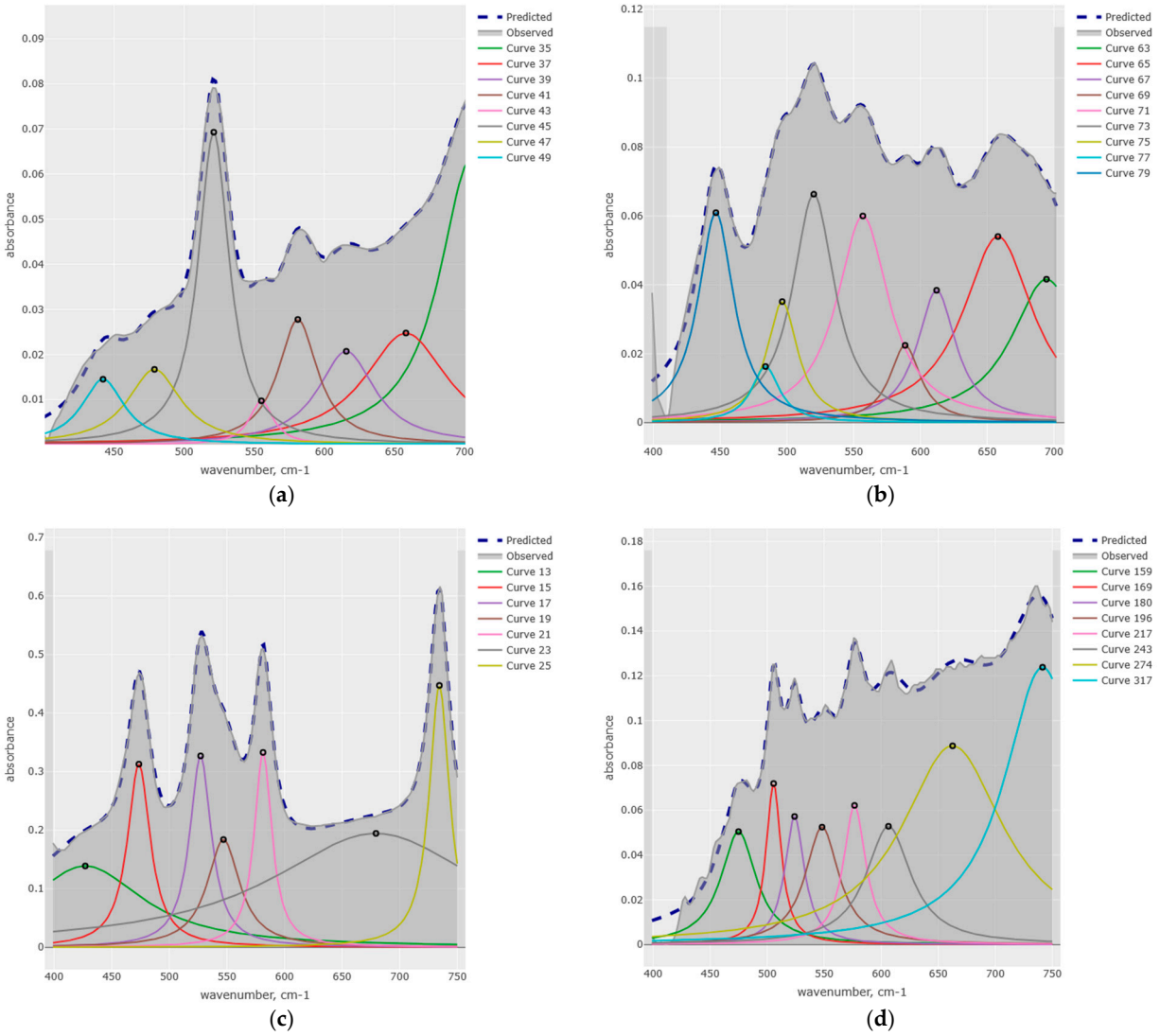


Figure 6. IR spectra of (**a**) [2.2]; (**b**) product of [2.2] + $H[AuCl_4]$; (**c**) [2.2.2]; (**d**) [2.2.2] + $H[AuCl_4]$ fitted by Lorentzian curves in the range of 750 to 400 cm^{-1}.

A similar pattern was observed for the cryptand [2.2.2]. The spectrum of the free ligand was fitted with seven Lorentzian peaks at 426.1, 473.5, 527.3, 547.8, 581.4, 677.2, and 734.5 cm^{-1}. In contrast, the spectrum of its gold(III) complex required eight components, with fitted maxima at 475.0, ***505.7***, 523.9, 548.0, 576.5, ***606.4***, 662.2, and 741.4 cm^{-1}. Again, the majority of these bands are common to both the free and complexed ligand, but a new vibration at ***505.7*** cm^{-1} emerges exclusively in the complex, providing further evidence for metal–nitrogen coordination. In general, we consider peaks that differ by no more than 10 cm^{-1} to be substantially the same, taking into account the experimental error in their determination, the spectral resolution, and the standard deviation of the optimization procedure.

To support the assignment of the new IR bands observed in the complexes, it is instructive to consider the characteristic vibration frequencies for gold–ligand bonds. The stretching vibrations of the Au–Cl bond typically fall outside the spectral range accessible with our instrument, appearing at lower wavenumbers (340 to 370 cm^{-1}), with the exact value depending on the counterion and the nature of the other ligands in the coordination sphere, as established by both experimental [44] and theoretical [41,42] studies.

In contrast, our quantum chemical calculations provide a clear benchmark for the Au–N vibration [42]. For example, the antisymmetric Au–N stretching mode in the model

complex *trans*-$[AuCl_2(NH_3)_2]^+$ was calculated to appear at 539.1 cm^{-1}, while in other complexes this band typically appeared at 530 to 550 cm^{-1}. On the basis of these computational benchmarks, the new absorption bands observed experimentally at approximately 500 cm^{-1} for the cryptand complexes can be assigned to the Au–N stretching mode. The slight shift to a lower wavenumber compared to the ammine complex is consistent with the coordination of a heavier tertiary amine nitrogen (from the cryptand) rather than the lighter ammonia molecule.

Furthermore, the fitting analysis also revealed a Lorentzian component at approximately 600 cm^{-1} in spectrum of the complex with [2.2.2]. Based on previous theoretical work [41,42], this band may be tentatively assigned to an Au–O stretching vibration, suggesting possible coordination through the oxygen atoms of the macrocycle in addition to the nitrogen donors.

2.3.3. ^{1}H NMR Spectral Data

^{1}H NMR spectroscopy is a particularly valuable tool for distinguishing between inclusion (inner) and exclusion (outer) complexes of cryptands. When a metal ion is encapsulated within the cryptand cavity (inner complex), its exchange with the bulk solution is typically slow on the NMR timescale, even for otherwise labile cations. This slow exchange results in separate, distinct sets of signals for the free and complexed ligand, rather than a single averaged signal. This phenomenon has been well documented, for example, in the spectra of Ba^{2+} with [2.2.2] [45] and Na^+ or Li^+ with the [1.1.1] cryptand [46].

Conversely, if inner-sphere complexation is prevented (for instance, by a mismatch between the ionic radius of the metal and the cavity size) the exchange between free and bound ligand is rapid. Under these conditions, the NMR signals coalesce into an averaged set of resonances. This behavior is observed for K^+ complexes with [2.2.2] [45,46], where the larger potassium ion does not fit optimally inside the cavity. In a particularly illustrative example, ^{133}Cs NMR spectroscopy was used to identify both inclusion and exclusion-type complexes of Cs^+ with [2.2.2] in the same solution, demonstrating the coexistence of slow and fast exchange regimes depending on the binding mode [47].

However, the kinetic lability of the metal complex itself must also be considered. Gold(III) complexes are generally considered to be inert. Even in the parent tetrachloroaurate(III) ion, chloride exchange with the bulk solution is relatively slow, with reported half-times ranging from 0.7 to 4.2 min, depending on Cl^- concentration and temperature [48]. This inertness extends to mixed-ligand complexes; chloride exchange is hindered [49], and NMR spectra indicate slow exchange for complexes with S-donor ligands such as cysteine [50] and dithiocarbamate [51]. Complexes with N-donor ligands are also generally reported to be inert [52]; for example, ammonia exchange in tetraamminegold(III) is slow [53].

In contrast, gold(III) complexes with O-donor ligands appear to be significantly more labile, as inferred from several indirect lines of evidence. For instance, the hydroxide ligand in a gold(III) complex with diethylenetriamine undergoes very rapid exchange with Br^- [54]; $[AuCl_3(H_2O)]$ oxidizes tetracyanoplatinate(II) much faster than does $[AuCl_4]^-$ [55]; it has been suggested that tetrachloroaurate(III) must undergo two successive hydrolysis steps before it can bind to DNA [56]; and the exchange of two different O-donor bidentate ligands in a gold(III) complex has been described as instantaneous [57].

This distinct kinetic behavior provides a powerful diagnostic tool for interpreting the NMR spectra of our systems. We can therefore formulate the following expectations: slow exchange (manifesting as separate signals for free and bound ligand) would be indicative of either inner-sphere complexation (metal encapsulated in the macrocyclic cavity) or, at a minimum, coordination through nitrogen donor atoms. At the same time, fast exchange

(manifesting as a single set of averaged signals) would suggest exclusion-type coordination or binding through oxygen atoms.

Furthermore, beyond the exchange regime, the extent of the chemical shift displacement upon complexation, as well as any increase in the number of signals (which would indicate a lowering of molecular symmetry), can provide additional structural information about the gold(III) complexes.

The ^{1}H NMR spectra of D_2O solutions of the free macrocyclic ligands, as well as their mixtures with $HClO_4$ and $H[AuCl_4]$, are presented in Figures 7 and S3.

The ^{1}H NMR spectra of the free macrocycles recorded in this study are in good agreement with previously reported data for 18C6 [58], 1N18C6 [59]; [2.2] [60] (in D_2O), [61] (in $CDCl_3$); [2.2.2] [62] (in $CDCl_3$), [63] (in methanol). The key spectral features are given in Table S2. In particular, 18C6 spectrum exhibits a single singlet at 3.61 ppm, corresponding to its 12 equivalent methylene groups (2 H in each). The spectrum of 1N18C6 displays a more complex pattern due to the presence of the nitrogen atom. Multiplets are observed at 2.73 ppm (assigned to the –NH–**CH$_2$**–CH$_2$–O– protons) and 3.58 ppm (assigned to the –NH–CH$_2$–**CH$_2$**–O– protons). A doublet at 3.60 ppm accounts for all other methylene fragments. Both [2.2] and [2.2.2] cryptands show three distinct resonances. For [2.2], these appear at 2.70 ppm (–NH–**CH$_2$**–CH$_2$–O–), 3.55 ppm (–NH–CH$_2$–**CH$_2$**–O–), and 3.57 ppm (–O–**CH$_2$**–**CH$_2$**–O–). For [2.2.2], the corresponding resonances are found at 2.79 ppm, 3.59 ppm, and 3.56 ppm.

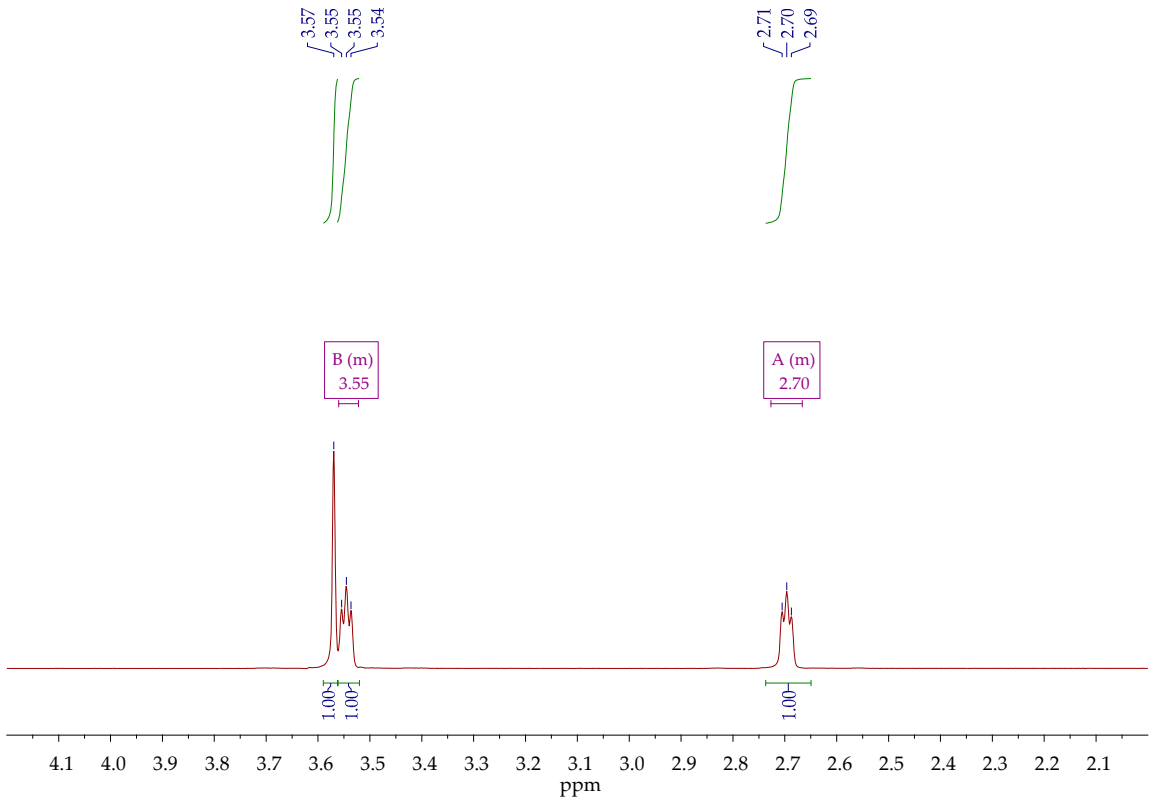
As expected, protonation of the ligands has a pronounced effect on the NMR spectra, particularly on the signals of methylene groups adjacent to the nitrogen atoms. For example, upon addition of $HClO_4$ to [2.2] (Figure 7a,b), the resonances for the –NH–**CH$_2$**–CH$_2$–O– protons shift downfield from 2.70 to 3.05 ppm, and those for the –NH–CH$_2$–**CH$_2$**–O– shift downfield from 3.55 to 3.64 ppm. In contrast, the signal for the –O–**CH$_2$**–**CH$_2$**–O– protons, which are further from the protonation site, remains almost unchanged (3.57 to 3.60 ppm). This deshielding is expected, as the introduction of an additional positive charge (the proton) withdraws electron density from the neighboring functional groups. The correctness of the spectral assignment is confirmed by {^{1}H, ^{1}H} COSY NMR spectra that show cross-correlation between multiplets referring to –NH–**CH$_2$**–CH$_2$–O– and –NH–CH$_2$–**CH$_2$**–O– protons for 1N18C6 and [2.2] (Figure S4).

An attempt to isolate the monoprotonated form of [2.2.2] was unsuccessful. At an equimolar ratio of strong acid to ligand, a mixture of $H[2.2.2]^+$ and $H_2[2.2.2]^{2+}$ was obtained (Figure S3b). The fully protonated species, $H_2[2.2.2]^{2+}$, could be clearly observed only upon the addition of an excess of perchloric acid (Figure S3c).

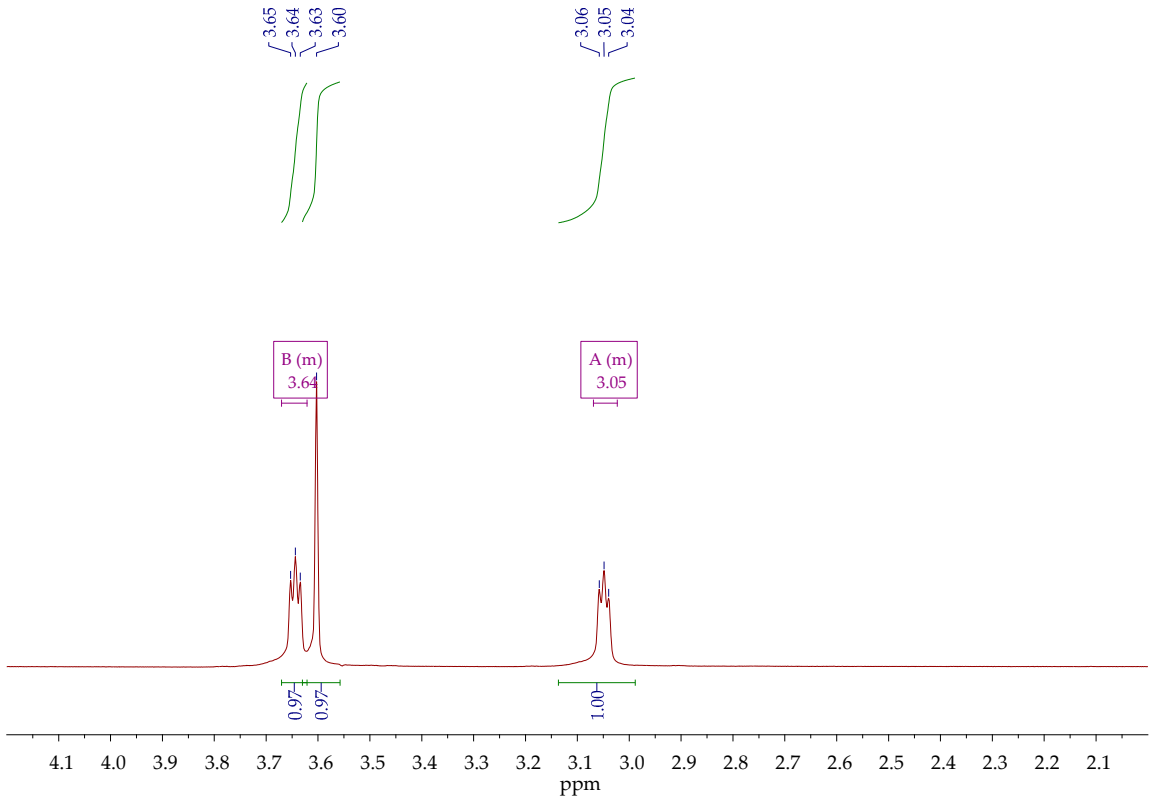
The addition of $H[AuCl_4]$ to solutions of the macrocycles results in the formation of both protonated ligand species and gold(III) complexes. The spectral manifestations of this complexation vary significantly depending on the ligand structure. Remarkably, no changes were observed in the ^{1}H NMR spectrum of the 18C6 + $H[AuCl_4]$ mixture compared to the free ligand (Figure S3g,i). While it is known that complexation of 18C6 typically induces only small shifts in its singlet resonance (on the order of tenths [64] or even hundredth [65] of a ppm; sometimes, the changes are so small that they are measured in Hz instead of ppm [66]); the shift in our case was as small as ~0.5 Hz. Furthermore, the absence of signal splitting indicates that the ligand exchange between the free and complexed states is fast on the NMR timescale.

The spectrum of [2.2] mixture with $H[AuCl_4]$ (Figure 7c) shows a set of signals with a relative integral intensity (RIE) of 1.0, assigned to the $H[2.2]^+$ species. These appear as two multiplets at 3.20 and 3.68 ppm and a singlet at 3.61 ppm, which correspond closely to the protonated ligand spectrum in Figure 7b. An additional set of signals with an RIE of ~0.4 is

observed and tentatively assigned to the $[AuCl_{4-n}[2.2]]^{n-1}$ complex. This set consists of five multiplets (2.77 dd, 2.97 ddd, 3.31 ddd, 3.86 ddd, 4.01 dd) and a singlet at 3.74 ppm.

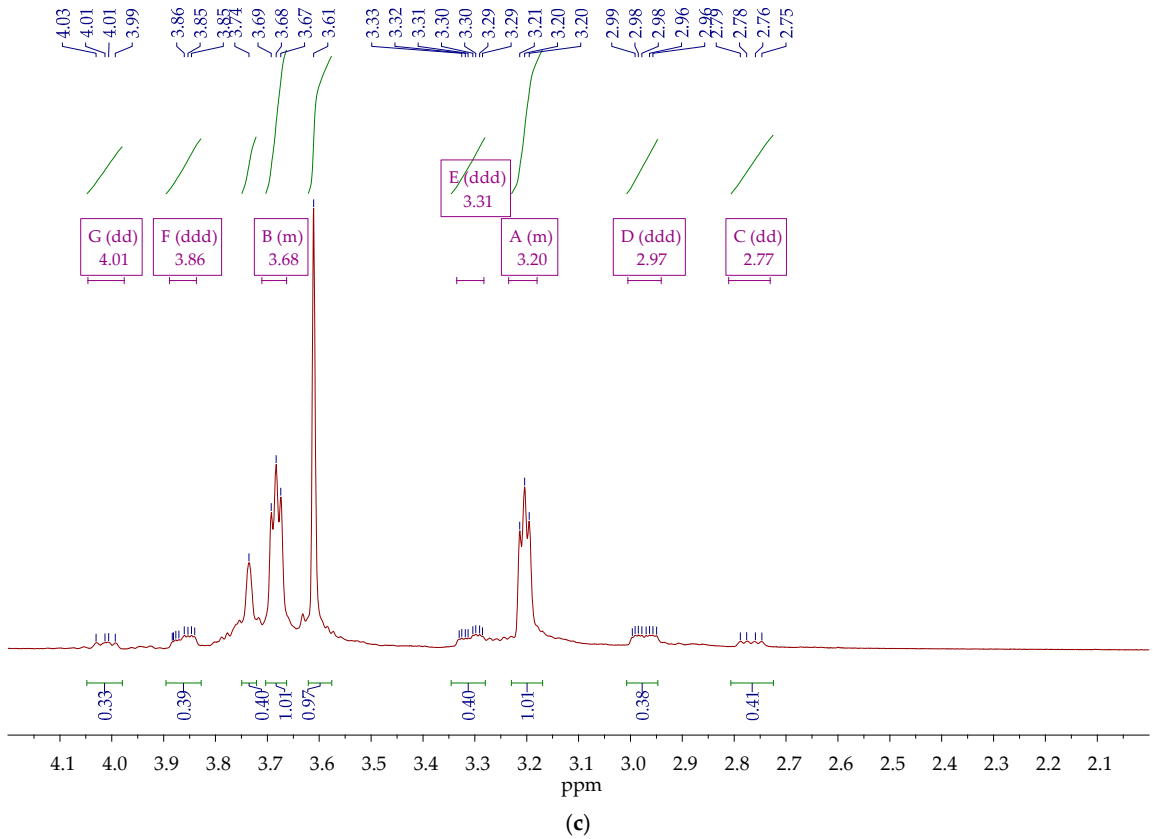


(**a**)



(**b**)

Figure 7. *Cont.*



(**c**)

Figure 7. ^{1}H NMR spectra of D_2O solutions of: (**a**) [2.2] (0.01 M); (**b**) [2.2] (0.01 M) + $HClO_4$ (0.01 M); (**c**) [2.2] (0.01 M) + H[$AuCl_4$] (0.005 M).

The spectrum of 1N18C6 mixture with H[$AuCl_4$] (Figure S3g) is even more complex. In addition to the resonances of the protonated ligand (3.22, 3.62, 3.71 ppm; RIE 1.0; see Figure S3f), two minor sets of signals can be discerned. The first set (RIE ~0.3) appears at 2.91, 3.00, 3.55, 3.59, and 3.77 ppm, and is tentatively assigned to the 1:1 complex, [$AuCl_{4-n}$(1N18C6)]$^{n-1}$. The second, even weaker set (RIE ~0.18) at 3.14, 3.38, 3.44, 4.11, and 4.17 ppm, may correspond to the *bis*-ligand complex, [$AuCl_{4-n}$(1N18C6)$_2$]$^{n-1}$.

The spectrum of [2.2.2] mixture with H[$AuCl_4$] (Figure S3d) is the most intricate. It clearly shows signals for the monoprotonated HL^+ (2.92, 3.58, 3.61 ppm; RIE 1.0; see Figure S3b for comparison) and diprotonated H_2L^{2+} species (3.47, 3.65, 3.79 ppm; RIE ~0.75; see Figure S3b,c for comparison). In addition, two distinct groups of complex signals are observed. A pair of relatively intense multiplets at 3.15 and 3.38 ppm (RIE ~0.17) is tentatively assigned to an inner-sphere [$AuCl_{4-n}$[2.2.2]]$^{n-1}$ complex, where the metal is encapsulated within the cryptand cavity. A set of six very weak resonances (2.46, 2.60, 2.69, 3.21, 3.71, 3.93 ppm; RIE approaching 0) is attributed to outer-sphere complexes, most likely the tetraligand species [Au([2.2.2])$_4$]$^{3+}$. Since accommodating four ligands around a single gold(III) center in an inner-sphere mode is sterically impossible, the observation of these weak, complex signals provides support for the existence of outer-sphere coordination, where the cryptands bind to the metal through the periphery rather than encapsulation. Since the outer coordination is the only viable option of four ligand accommodation around gold(III) cation, the complexes with other ligands showing multiple resonances in ^{1}H NMR spectra should take similar coordinating mode.

A summary of the proposed signal assignments and the corresponding tentative complexes' structure supported by the spectral evidence is presented in Table 3.

Table 3. Tentative structure of gold(III) complexes with macrocyclic ligands with the experimental evidence.

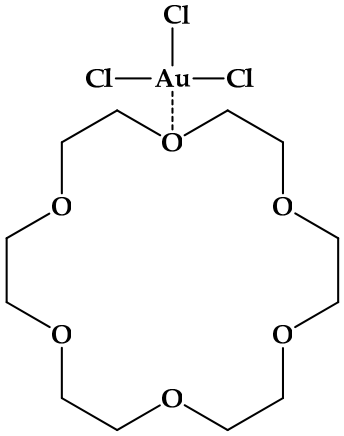
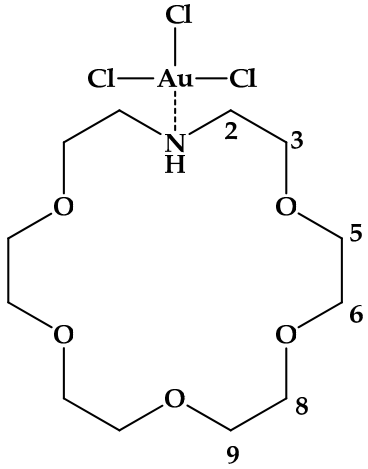
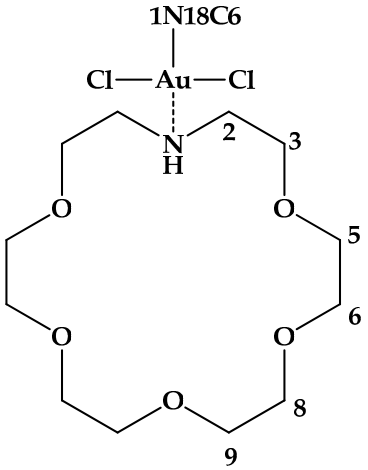
Structure	Experimental Evidence	Notes
 [$AuCl_3$18C6]	Changes in UV-Vis spectra upon H[$AuCl_4$] titration by 18C6; ^{1}H NMR peaks: 3.61	Fast chemical exchange on the NMR timescale, consistent with coordination through labile oxygen donor atoms. This results in signal averaging between free and complexed ligand, and no distinct resonances for the complex are observed. Perhaps, the low equilibrium concentration of the complex, predicted by its relatively small stability constant (log β = 4.52), might contribute to the absence of detectable complex signals in the ^{1}H NMR spectrum.
 [$AuCl_3$1N18C6]	Changes in E.M.F. upon 1N18C6 titration by H[$AuCl_4$]; Changes in UV-Vis spectra upon H[$AuCl_4$] titration by 18C6; ^{1}H NMR peaks: 2.91 (2), 3.00 (3), 3.55 (5), 3.56 (6), 3.77 (8)	Slow chemical exchange on the NMR timescale, consistent with coordination through the nitrogen donor atom. Five of the six expected signals for this complex are resolved; the missing resonance is likely obscured by overlap with the more intense signals of the protonated ligand. The proposed structure is supported by the close similarity between the UV-Vis spectra of the 1N18C6 and 18C6 complexes (Figure 5), suggesting analogous coordination geometries despite the difference in exchange kinetics.
 [$AuCl_2$(1N18C6)$_2$]$^+$	Changes in E.M.F. upon 1N18C6 titration by H[$AuCl_4$]; Changes in UV-Vis spectra upon H[$AuCl_4$] titration by 18C6; ^{1}H NMR peaks: 3.14 (2), 3.38 (3), 3.44 (5), 4.11 (6), 4.17 (8)	Slow chemical exchange on the NMR timescale, consistent with coordination through nitrogen donor atoms. Five of the six expected signals for this complex are resolved; the missing resonance is likely obscured by overlap with signals from the protonated ligand species. Compared to the monoligand complex, the resonances of the *bis*-ligand species are shifted further downfield. This deshielding is attributed to the increased positive charge on the complex upon substitution of a second anionic chloride ligand by a neutral 1N18C6 molecule, which enhances the electron-withdrawing effect on the ligand protons.

Table 3. *Cont.*

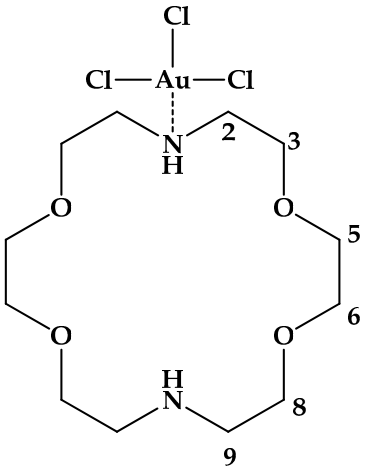
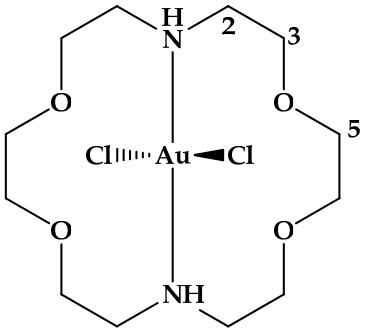
Structure	Experimental Evidence	Notes
 [$AuCl_3$[2.2]]	Changes in E.M.F. upon [2.2] titration by H[$AuCl_4$]; ^{1}H NMR peaks: 2.77 (2), 2.97 (3), 3.31 (5), 3.74 (6), 3.86 (8), 4.01 (9)	Slow chemical exchange on the NMR timescale, consistent with coordination through nitrogen donor atom(s). The existence of this species is supported by the similarity between its formation constant and that of the 1N18C6 monoligand complex (Table 2), suggesting analogous binding modes. However, a discrepancy arises when comparing the UV-Vis data. Unlike the 1N18C6 complex, the UV-Vis spectrum of the [2.2] species does not closely resemble that of the 18C6 complex (Figure 5), as might be expected for a simple monoligand structure. This apparent inconsistency may be reconciled by considering the significantly different concentration regimes of the two techniques. The NMR and potentiometric experiments were conducted at relatively high total reagent concentrations, favoring the formation and detection of the 1:1 complex. In contrast, the much lower concentrations used in the UV-Vis titration may shift the equilibria towards formation of inclusion complexes (*vide infra*), leading to a negligible concentration of this particular species under those conditions, which would explain its spectral features not being prominently observed.
 [$AuCl_2$[2.2]]$^+$	Changes in UV-Vis spectra upon H[$AuCl_4$] titration by [2.2]; Precipitation in the end of potentiometric titration; IR-spectra of the precipitated product; ^{1}H NMR peaks: Not observed.	It must be acknowledged that this proposed structure is not directly corroborated by the ^{1}H NMR data, as no distinct signals characteristic of such a species are observed in solution under the conditions of the NMR experiment. This may indicate that the complex is not the predominant species in solution or that its formation is concentration-dependent (see note for the [2.2] exclusion-type complex above). Despite the NMR discrepancy, several independent lines of evidence support the formation of this inclusion complex under specific conditions: 1. UV-Vis spectroscopy: The UV-Vis spectrum of the such [2.2] complex should be blue-shifted relative to those of the 18C6 and 1N18C6 complexes, which is observed in Figure 5. This hypsochromic shift is consistent with a higher degree of chloride substitution; coordination through both nitrogens would result in the displacement of two chlorides, rather than one, leading to a greater change in the ligand field and a more pronounced blue shift. Notably, the spectrum closely resembles that of the [2.2.2] complex, suggesting a similar coordination mode. 2. Protonation behavior: The unusually low protonation constant of the [2.2] complex (Section 2.2) is readily explained if both nitrogen atoms are involved in metal coordination and are thus unavailable for protonation. 3. IR spectroscopy: The solid product that precipitates at the end of the potentiometric titration exhibits a new IR absorption band at ~497 cm^{-1} (Figure 6), which is confidently assigned to an Au–N stretching vibration, providing direct evidence for nitrogen–gold coordination in the isolated material. 4. A structurally analogous palladium(II) complex with a similar cryptand has been isolated and its inclusion geometry unambiguously confirmed by X-ray diffraction [34].

Table 3. *Cont.*

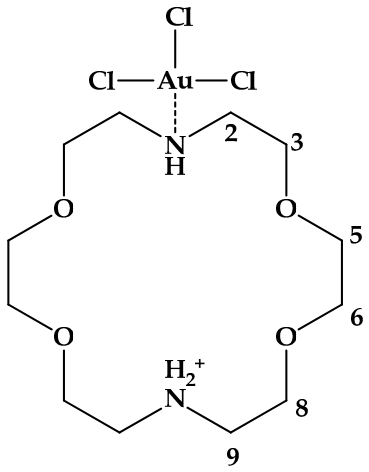
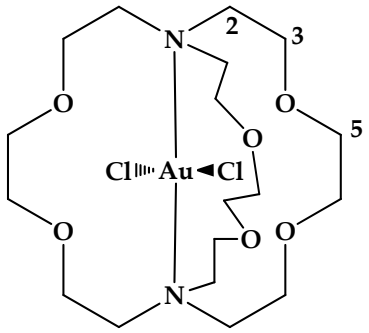
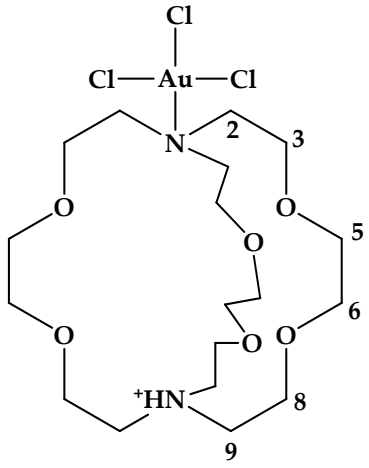
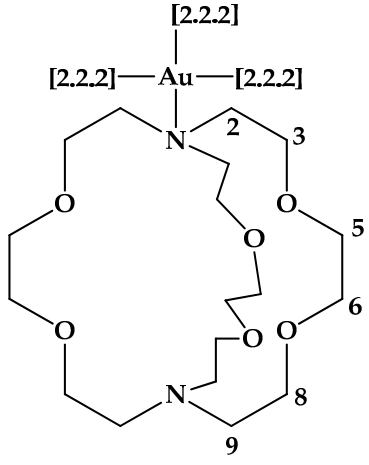
Structure	Experimental Evidence	Notes
 $[AuCl_3H[2.2]]^+$	Changes in E.M.F. upon 1N18C6 titration by $H[AuCl_4]$ (weak as the hypothesis about this species formation is not necessary for fitting experimental data); ^1H NMR peaks: Not observed.	A hypothetical and likely unstable species. Protonation of the coordinated cryptand would require protonation of a nitrogen atom, but both nitrogen donors are presumably involved in metal coordination in the inclusion complex (*vide supra*). Therefore, protonation would necessitate a significant structural rearrangement, potentially disrupting the gold–nitrogen bonds and/or leading to the re-entry of a chloride ion into the coordination sphere. This instability is consistent with the very low equilibrium concentration of this species inferred from the potentiometric data and the inability to detect it spectroscopically.
 $[AuCl_2[2.2.2]]^+$	Changes in E.M.F. upon [2.2.2] titration by $H[AuCl_4]$; Changes in UV-Vis spectra upon $H[AuCl_4]$ titration by 18C6; Precipitation in the end of potentiometric titration; IR-spectra of the precipitated product; ^1H NMR peaks: 3.15 (2), 3.38 (3)	Slow chemical exchange on the NMR timescale, consistent with coordination through nitrogen donor(s) and the formation of an inner-sphere (inclusion) complex. Of the three expected signals for this complex, only two are clearly resolved; the third is likely obscured by overlap with the more intense resonances of protonated ligand species. A preponderance of evidence from multiple independent techniques supports the formation of this inclusion complex: 1. The UV-Vis spectrum of this [2.2.2] complex should be blue-shifted relative to those of the 18C6 and 1N18C6 complexes, which is observed in Figure 5. This hypsochromic shift is consistent with a higher degree of chloride substitution; coordination through both nitrogen atoms would result in the displacement of two chlorides, leading to a greater change in the ligand field. Notably, the spectrum closely resembles that of the [2.2] inclusion complex, suggesting analogous coordination modes for the two cryptands. 2. The unusually low protonation constant of the [2.2.2] complex (Section 2.2) is readily explained if both nitrogen atoms are involved in metal coordination and are thus unavailable for protonation. 3. The higher equilibrium constant for chloride substitution by [2.2.2] compared to the other ligands (Table 2) reflects the enhanced stability conferred by the cryptand architecture. The absence of a pronounced chelate effect (i.e., $\log \beta < 2 \log \beta_{Cl/NH3}$) does not contradict this assignment; it may be attributed to steric constraints associated with accommodating two bulky chloride ligands within the cryptand cavity alongside the metal ion. 4. The solid product that precipitates at the end of the potentiometric titration exhibits a new IR absorption band at ~506 cm^{-1} (Figure 6), which is confidently assigned to an Au–N stretching vibration, providing direct evidence for nitrogen–gold coordination in the isolated material. 5. A structurally analogous palladium(II) complex with a similar cryptand has been isolated and its inclusion geometry unambiguously confirmed by X-ray diffraction [34] providing a precedent for the proposed coordination mode.

Table 3. *Cont.*

Structure	Experimental Evidence	Notes
 $[AuCl_3H[2.2.2]]^+$	Changes in E.M.F. upon [2.2.2] titration by $H[AuCl_4]$; Changes in UV-Vis spectra upon $H[AuCl_4]$ titration by 18C6; ^{1}H NMR peaks: Not observed.	An unstable species. Protonation of the coordinated cryptand would require protonation of a nitrogen atom, but both nitrogen donors are presumably involved in metal coordination in the inclusion complex (*vide supra*). Therefore, protonation would necessitate a significant structural rearrangement, potentially disrupting the gold–nitrogen bonds and/or leading to the re-entry of a chloride ion into the coordination sphere. This instability is consistent with the low equilibrium concentration of this species inferred from the potentiometric data. This species may show the UV-Vis spectrum similar to those of complexes with 18C6 and 1N18C6 (Figure 5).
 $[Au[2.2.2]_4]^{3+}$	Changes in E.M.F. upon [2.2.2] titration by $H[AuCl_4]$; Changes in UV-Vis spectra upon $H[AuCl_4]$ titration by 18C6; ^{1}H NMR peaks: 2.46 (2), 2.60 (3), 2.69 (5), 3.21 (6), 3.71 (8), 3.93 (9)	Slow chemical exchange on the NMR timescale, consistent with coordination through nitrogen donor atoms in an outer-sphere (exclusion) mode, where four cryptand molecules surround the central gold(III) ion without encapsulation. Unlike the monoligand inclusion complexes, several resonances in the ^{1}H NMR spectrum of this species are shifted upfield relative to the free cryptand. This is in contrast to the downfield shifts typically observed upon protonation or metal coordination (which withdraw electron density). The observed upfield shift may be explained by effective delocalization of the positive charge over the four bulky, electron-rich ligands surrounding the metal center. This charge delocalization could increase the local electron density on the ligand protons, resulting in greater shielding and an upfield shift. The UV-Vis spectrum of this complex exhibits the most pronounced hypsochromic (blue) shift of all species studied (Figure 5). This is consistent with the proposed structure, in which all four chloride ligands have been completely substituted by nitrogen-donor macrocycles. The resulting coordination sphere, composed entirely of nitrogen donors, is analogous to that of the well-characterized tetraamminegold(III) complex, $[Au(NH_3)_4]^{3+}$, and the observed spectrum (Figure 4) is in good agreement with literature data for that compound [40].

2.4. Weaknesses and Limitations of This Study

While this study provides a comprehensive thermodynamic and spectroscopic characterization of gold(III) complexes with a series of macrocyclic ligands, several limitations and unresolved questions should be acknowledged. Addressing these points will be the focus of future investigations. In general, spectra (including UV-Vis, IR and NMR) cannot be unambiguously assigned without the high-level theoretical calculations that support the experimental findings.

2.4.1. The 18C6 Complex

Although the UV-Vis spectra of tetrachloroaurate(III) show clear changes upon the addition of 18C6 (this variation cannot be attributed to protolytic equilibria, as 18C6 is neither an acid nor a base), the absence of any detectable shift in the ^{1}H NMR spectrum of 18C6 upon H[$AuCl_4$] addition remains puzzling. This discrepancy likely arises from a combination of factors: the low equilibrium concentration of the complex (consistent with its small stability constant), the fast exchange regime typical of O-donor ligands, and the very small chemical shift changes expected for this system. A definitive understanding of this complex will require its isolation and structural characterization in the crystalline phase, which is a goal for future work.

2.4.2. The [2.2] Complex

The structural assignment for the gold(III) complex with cryptand [2.2] is the most challenging and carries the greatest uncertainty. Two lines of evidence support the formation of an inclusion complex under some conditions: the UV-Vis spectrum of the species closely resembles that of the [2.2.2] inclusion complex, and the very low protonation constant of the complex suggests that both nitrogen atoms are involved in metal coordination. However, other observations are more consistent with an exclusion-type structure under the conditions of the NMR and potentiometric experiments (i.e., at higher reagent concentrations). In particular, the close similarity between the formation constants of the [2.2] and 1N18C6 complexes (Table 2) suggests analogous, monodentate binding modes. The resonances observed in the experimental ^{1}H NMR spectrum indicate the significant decrease in ligand symmetry, which also support the outer type of complex.

This apparent contradiction may indicate that the coordination mode of [2.2] is concentration-dependent, or that multiple species coexist in solution. To resolve this ambiguity, advanced structural techniques such as EXAFS/XANES spectroscopy would be invaluable. These methods could provide direct, element-specific information about the local coordination environment of the gold(III) center, definitively establishing the number of nitrogen and chloride ligands in its immediate vicinity.

3. Materials and Methods

3.1. Chemicals

The following macrocyclic ligands were used as received without further purification: 18-crown-6 (18C6, Acros Organics, Ankleshwar, Gujarat, India, claimed purity > 99%), 1-aza-18-crown-6 (1N18C6, Macklin, Shanghai, China, claimed purity $\geq$ 98.0%), and the cryptands [2.2] and [2.2.2] (both from Merck, Darmstadt, Germany, claimed purity $\geq$ 99.0%). Hydrogen tetrachloroaurate(III) trihydrate, H[$AuCl_4$]·3H_2O (Aurat, Moscow, Russia, claimed gold mass fraction 49.11%), was also used without additional purification.

Perchloric acid ($HClO_4$) was standardized by titration against a standardized solution of sodium tetraborate decahydrazte ($Na_2B_4O_7$·10H_2O) using methyl orange as an indicator. Both reagents were sourced from Reakhim (Staraya Kupavna, Russia).

All aqueous solutions were prepared using deaerated bidistilled water (specific conductivity κ = 3.6 $\mu S \cdot cm^{-1}$, pH 6.0). Deuterium oxide (D_2O, 99.8% isotope purity), used as the solvent for NMR spectroscopy, was purchased from Carl Roth GmbH (Karlsruhe, Germany).

3.2. Potentiometric Titration

Potentiometric titrations were performed to determine both the protonation constants of the ligands and the stability constants of their gold(III) complexes.

For the determination of complex formation constants, an aliquot (20.00 mL) of an aqueous solution of the macrocyclic ligand (1N18C6: 0.002935 M; [2.2]: 0.002627 M; [2.2.2]: 0.002183 M) was titrated with an aqueous solution of $H[AuCl_4]$ (0.1006 M). Titrant was added in 40 µL increments, and 20 to 30 data points were acquired for each experiment.

For the determination of ligand protonation constants, separate titrations were performed. Aliquots of the macrocycle solutions at the same concentrations (see above) were titrated with a standard $HClO_4$ solution (1.1751 M), added in 5 µL increments to acquire approximately 20 data points per experiment.

All titrations were carried out in the absence of any supporting electrolyte. The maximum ionic strength reached during the experiments, due solely to the added $H[AuCl_4]$, did not exceed 0.006 M.

The EMF of the solutions was measured using an I-160MI pH-meter/millivoltmeter (Izmeritel'naya Tekhnika, Moscow, Russia) equipped with a combined pH-sensitive microelectrode (InLab Pro, Mettler Toledo, Greifensee, Switzerland) and a TDL-1000-06 temperature sensor (Izmeritel'naya Tekhnika, Moscow, Russia). Prior to each set of experiments, the potentiometric setup was calibrated using a series of buffer solutions with pH values of 1.65, 4.01, 6.86, 9.18, and 12.43, prepared from standard samples (Uralkhiminvest, Ufa, Russia). This calibration procedure is suitable for solutions with ionic strengths ≤ 0.1 M [67]. The standard electrode potential (464.77 mV) and Nernstian slope (-58.7 mV·pH^{-1}) obtained from the calibration were used to calculate equilibrium constants from the experimental titration data.

3.3. UV-Vis Titration

UV-Vis spectrophotometric titrations were performed as an independent method to validate the complex formation constants and to characterize the electronic spectra of the individual complex species.

An aliquot (2.52 mL) of an aqueous $H[AuCl_4]$ solution (1.229×10^{-4} M) was placed in a quartz cuvette and titrated with aqueous solutions of the macrocyclic ligands: 18C6 (0.002983 M), 1N18C6 (0.002935 M), [2.2] (0.002627 M), and [2.2.2] (0.002183 M). The titrant was added in 5 µL increments, and 25 to 30 data points were acquired for each experiment. All titrations were carried out in the absence of any supporting electrolyte. The maximum ionic strength reached during the experiments, due solely to the $H[AuCl_4]$ present, did not exceed 0.0002 M.

UV-Vis spectra were recorded over the wavelength range of 200 to 400 nm (absorbance range 0 to 3 log units) using a UV1800 spectrophotometer (Shimadzu, Canby, OR, USA). Standard quartz cells with an optical path length of 1.00 cm were used for all measurements.

Both potentiometric and UV-Vis experiments were performed under ambient atmospheric pressure at a temperature of 298.2 ± 0.1 K, maintained using an external water-circulating thermostat.

3.4. Experimental Data Processing

The equilibrium constants for all the reactions of ligand substitution occurring in solution were calculated from the potentiometric and spectrophotometric titration data using the KEV freeware package (ver. 0.6.0) [68].

The following equilibria were included in the overall chemical model for each system: (a) successive protonation constants for each ligand were considered (one for 1N18C6, two for [2.2] and [2.2.2]), as determined independently in this work (see Section 2.1 and Table 1); (b) the hydrolysis of tetrachloroaurate(III) was accounted for using the literature values for the stepwise hydrolysis constants: $\log K_{H1} = -6.1$ and $\log K_{H2} = -13.2$ [38,69]); (c) The ionic product of water was fixed at $\log K_w = -14.0$ [70]; (d) the formation of gold(III) complexes

with the macrocyclic ligands, with various stoichiometries, was modeled as described in Section 2.2. The refined stability constants for the proposed species are presented in Table 2.

The KEV software was used to refine the stability constants by minimizing the sum of squared residuals between the calculated and experimental EMF or absorbance values, based on the specified chemical model.

3.5. IR Spectroscopy

The products precipitated from the mixture of ligands [2.2] and [2.2.2] with $H[AuCl_4]$ after finishing potentiometric titrations were collected on a glass filter and washed with water trice. Then the precipitates were dried in dessicator over $CaCl_2$. The samples for IR spectroscopy were prepared *via* fine dispersing of a mixture of free ligands and precipitation products with KBr used as matrix.

Infrared spectra of the free cryptands [2.2] and [2.2.2], as well as the solid products obtained from their reaction mixtures with $H[AuCl_4]$, were recorded using an Avatar 360 FTIR spectrometer (Thermo Nicolet, Sugarland, TX, USA). The samples were prepared as KBr pellets. Spectra were collected over the wavenumber range of 4000 to 400 cm^{-1} with a spectral resolution of 2 cm^{-1}. The positions of the absorption bands were determined with an accuracy of ± 2 cm^{-1}.

3.6. ^1H NMR Spectroscopy

^1H NMR spectra were recorded using a Bruker Avance III 500 NMR spectrometer (Bruker, Mannheim, Germany) operating at a ^1H frequency of 500.17 MHz. The temperature was maintained at 298.2 ± 0.1 K using a Bruker variable temperature unit (BVT-2000); samples were not spun during data acquisition. Chemical shifts were referenced to an external standard of hexamethyldisiloxane (HMDSO, Sigma Aldrich, MA, USA) and are reported with an accuracy of ±0.01 ppm.

Spectra were acquired using the standard pulse sequence [71] implemented in the TopSpin 3.6.1 software. The spectral window was set to 7183.9 Hz, and 32,768 data points (TD) were collected.

Stock solutions of each macrocyclic ligand (0.01 M) were prepared in D_2O. A 1.5 mL aliquot of each stock solution was then divided into three equal portions of 500 µL:

Sample A (control): No further additions.

Sample B (protonated ligand; except for 18C6, which does not accept protons): 5 µL of $HClO_4$ (1.1751 M) was added.

Sample C (gold(III) mixture): 25 µL of $H[AuCl_4]$ (0.1006 M) was added.

The prepared solutions were then transferred to standard 5 mm NMR tubes for analysis.

4. Conclusions

This study provides a comprehensive thermodynamic and spectroscopic characterization of the complexation between gold(III) and a series of macrocyclic ligands, *viz.* 18-crown-6 (18C6), 1-aza-18-crown-6 (1N18C6), 1,10-diaza-18-crown-6 ([2.2]), and the cryptand 4,7,13,16,21,24-hexaoxa-1,10-diazabicyclo[8.8.8]hexacosane ([2.2.2]) in aqueous solution at T = 298.2 K, p = 0.1 MPa, and $I \rightarrow 0$.

The stability constants for chloride substitution by these macrocycles reveal a clear trend: aza-substitution dramatically enhances the affinity for gold(III). The introduction of a single nitrogen atom (1N18C6) increases the stability constant by approximately 4.5 log units compared to the all-oxygen crown ether 18C6 (9.15 ± 0.03 vs. 4.52 ± 0.04 log units). The stoichiometry of the complexes becomes progressively more sophisticated with increasing nitrogen content and structural preorganization. While 18C6 forms only a 1:1 (ML) complex,

1N18C6 forms both ML and ML_2 species (log β_1 = 9.15 ± 0.03; log β_2 = 16.37 ± 0.09). The cryptand [2.2] forms ML (log β = 9.08 ± 0.07) and protonated MHL (log β = 12.99 ± 0.08) complexes, whereas [2.2.2] exhibits the richest speciation, forming ML (log β = 11.51 ± 0.08), MHL (log β = 15.90 ± 0.10), and an unusual tetraligand ML_4 (log β = 33.01 ± 0.28) complex.

The combination of UV-Vis, IR, and ^{1}H NMR spectroscopies provided insights into the structures of these complexes. In particular, addition of all macrocyclic ligands to tetrachloroaurate(III) solution results in bathochromic shift of both short wavelength maximum from 219 to 211 nm (with further shift to 202 nm in the case of [2.2.2] ligand), and long wavelength shoulder from 289 to ~285 nm. In the IR spectra of precipitated products of $H[AuCl_4]$ reaction with [2.2] and [2.2.2] cryptands, new peaks arise at 497 and 506 cm^{-1}, respectively, that can be assigned to Au-N stretching vibrations. The data indicate that 18C6 and 1N18C6 form exclusion-type complexes, where the gold(III) ion coordinates to the periphery of the macrocycle. In contrast, the cryptands [2.2] and [2.2.2] are capable of forming inclusion-type complexes, with the gold ion encapsulated within the macrocyclic cavity. For [2.2.2], this inclusion complex is the most stable species formed. However, the structural assignment for the [2.2] complex is less definitive, with potentiometric and UV-Vis data supporting an inclusion structure, while NMR spectra under the conditions of that experiment are more consistent with an exclusion-type binding mode. This discrepancy highlights the potential for concentration-dependent speciation and will be the focus of future investigations using techniques such as EXAFS/XANES.

The high stability constants determined for the aza-substituted macrocycles, particularly the cryptands, underscore their potential as practical agents for gold recovery and as receptor fragments in the design of chemosensors for this valuable metal.

Supplementary Materials: The following supporting information can be downloaded at: https://www.mdpi.com/article/10.3390/inorganics14040097/s1, Figure S1: Examples of potentiometric titration curves of 20 mL of: (a) 1N18C6 (0.002935 M); (b) [2.2] (0.002627 M); (c) [2.2.2] (0.002183 M) by $HClO_4$ (1.1751 M). Thirteen to twenty points were acquired in each experiment; V_{titr} = 5 µL. Points show the experimental E.M.F. values, while lines correspond to those calculated using the optimized equilibrium constants; Figure S2: IR spectra of cryptands [2.2] (a) and [2.2.2] (b) as well as products of their interaction with $H[AuCl_4]$; Figure S3: ^{1}H NMR spectra of D_2O solutions of: (a) [2.2.2] (0.01 M); (b) [2.2.2] (0.01 M) + $HClO_4$ (0.01 M); (c) [2.2.2] (0.01 M) + $HClO_4$ (0.02 M); (d) [2.2.2] (0.01 M) + $H[AuCl_4]$ (0.005 M); (e) 1N18C6 (0.01 M); (f) 1N18C6 (0.01 M) + $HClO_4$ (0.01 M); (g) 1N18C6 (0.01 M) + $H[AuCl_4]$ (0.005 M); (h) 18C6 (0.01 M); (i) 18C6 (0.01 M) + $H[AuCl_4]$ (0.005 M); Figure S4: {^{1}H, ^{1}H} COSY NMR spectra of protonated 1N18C6 (a) and [2.2] (b); Table S1: The most important IR vibrations of [2.2], [2.2.2] and their interaction product with $H[AuCl_4]$; Table S2: ^{1}H NMR spectra and signal assignment of crown esters as well as their protonated and complex species.

Author Contributions: Conceptualization, G.A.G.; methodology, M.N.Z. and G.A.G.; software, V.V.A. and G.A.G.; validation, D.N.Y., O.I.L., V.V.A. and M.N.Z.; formal analysis, V.V.A. and G.A.G.; investigation, D.N.Y., O.I.L., V.V.A., M.N.Z. and G.A.G.; resources, G.A.G.; data curation, G.A.G.; writing—original draft preparation, G.A.G.; writing—review and editing, M.N.Z. and G.A.G.; visualization, G.A.G.; supervision, G.A.G.; project administration, G.A.G.; funding acquisition, G.A.G. All authors have read and agreed to the published version of the manuscript.

Funding: This research was funded by Russian Science Foundation, grant number 22-73-10009-P, rscf.ru/project/22-73-10009-P/.

Institutional Review Board Statement: Not applicable.

Informed Consent Statement: Not applicable.

Data Availability Statement: Data is contained within the article or Supplementary Materials.

Conflicts of Interest: The authors declare no conflicts of interest.

Abbreviations

The following abbreviations are used in this manuscript:

18C6	18-crown-6
1N18C6	1-aza-18-crown-6
[2.2]	1,10-diaza-18-crown-6 (cryptand [2.2])
[2.2.2]	hexaoxa-1,10-diazabicyclo[8.8.8]hexacosan (cryptand [2.2.2])
RIE	relative integral intensity

References

1. Atwood, J.L. Inclusion (Clathrate) Compounds. In *Encyclopedia of Physical Science and Technology*; Elsevier: Amsterdam, The Netherlands, 2003; pp. 717–729.
2. Gokel, G.W.; Leevy, W.M.; Weber, M.E. Crown Ethers: Sensors for Ions and Molecular Scaffolds for Materials and Biological Models. *Chem. Rev.* **2004**, *104*, 2723–2750. [CrossRef]
3. Kryatova, O.P.; Korendovych, I.V.; Rybak-Akimova, E.V. Complexes of Benzo-15-Crown-5 with Protonated Primary Amines and Diamines. *Tetrahedron* **2004**, *60*, 4579–4588. [CrossRef]
4. Morrison, P.W.J.; Porfiryeva, N.N.; Chahal, S.; Salakhov, I.A.; Lacourt, C.; Semina, I.I.; Moustafine, R.I.; Khutoryanskiy, V.V. Crown Ethers: Novel Permeability Enhancers for Ocular Drug Delivery? *Mol. Pharm.* **2017**, *14*, 3528–3538. [CrossRef]
5. Chehardoli, G.; Bahmani, A. The Role of Crown Ethers in Drug Delivery. *Supramol. Chem.* **2019**, *31*, 221–238. [CrossRef]
6. Seyedi, S.M.; Sadeghian, A.; Sadeghian, H.; Hazrathoseyni, A.; Sadeghian, M. Synthesis and Biological Evaluation of Some New Thioether-Ester Crown Ethers. *Phosphorus Sulfur Silicon Relat. Elem.* **2007**, *182*, 265–272. [CrossRef]
7. Sadeghian, A.; Mohammad Seyedi, S.; Sadeghian, H.; Hazrathoseyni, A.; Sadeghian, M. Synthesis, Biological Evaluation and QSAR Studies of Some New Thioether–Ester Crown Ethers. *J. Sulfur Chem.* **2007**, *28*, 597–605. [CrossRef]
8. Hendrixson, R.R.; Mack, M.P.; Palmer, R.A.; Ottolenghi, A.; Ghirardelli, R.G. Oral Toxicity of the Cyclic Polyethers—12-Crown-4, 15-Crown-5, and 18-Crown-6—In Mice. *Toxicol. Appl. Pharmacol.* **1978**, *44*, 263–268. [CrossRef]
9. Arenaz, P.; Bitticks, L.; Pannell, K.H.; Garcia, S. Genotoxic Potential of Crown Ethers in Mammalian Cells: Induction of Sister-Chromatid Exchanges. *Mutat. Res. Genet. Toxicol.* **1992**, *280*, 109–115. [CrossRef]
10. Xavier, L.H.; Ottoni, M.; Abreu, L.P.P. A Comprehensive Review of Urban Mining and the Value Recovery from E-Waste Materials. *Resour. Conserv. Recycl.* **2023**, *190*, 106840. [CrossRef]
11. Kong, H.-Y.; Wang, T.-X.; Tao, Y.; Ding, X.; Han, B.-H. Crown Ether-Based Hypercrosslinked Porous Polymers for Gold Adsorption. *Sep. Purif. Technol.* **2022**, *290*, 120805. [CrossRef]
12. Fissaha, H.T.; Torrejos, R.E.C.; Kim, H.; Chung, W.-J.; Nisola, G.M. Thia-Crown Ether Functionalized Mesoporous Silica (SBA-15) Adsorbent for Selective Recovery of Gold (Au^{3+}) Ions from Electronic Waste Leachate. *Microporous Mesoporous Mater.* **2020**, *305*, 110301. [CrossRef]
13. Cai, A.; Yang, K.; Xu, L.; Li, M.; Zhang, W.; Yang, C.; Tian, Y.; Zhao, Z. Mechanistic Study of Selective Gold Extraction by Aza-Crown Ether. *Sep. Purif. Technol.* **2025**, *376*, 133974. [CrossRef]
14. Höffmann, L.; Blei, M.; Reissig, F.; Kopka, K.; Mamat, C. Preparation of Macrobicyclic Cryptands for Radiometal Complexation: Preparation of Macropa-Based Cryptands for Efficient Complexation of Radiometals. *Label. Compd. Radiopharm.* **2025**, *68*, e4136. [CrossRef] [PubMed]
15. Vasilikiotis, G.S.; Papadoyannis, I.N.; Kouimtzis, T.A. Analytical Applications of Crown Ethers. *Microchem. J.* **1984**, *29*, 356–360. [CrossRef]
16. Esteves, C.I.C.; Batista, R.M.F.; Raposo, M.M.M.; Costa, S.P.G. Novel Functionalised Imidazo-Benzocrown Ethers Bearing a Thiophene Spacer as Fluorimetric Chemosensors for Metal Ion Detection. *Dye. Pigment.* **2016**, *135*, 134–142. [CrossRef]
17. Pearson, R.G. Hard and Soft Acids and Bases, HSAB, Part 1: Fundamental Principles. *J. Chem. Educ.* **1968**, *45*, 581. [CrossRef]
18. Gamov, G.A. Complexation of Gold(I) and Gold(III) in Solutions. *Coord. Chem. Rev.* **2024**, *520*, 216162. [CrossRef]
19. Đurović, M.D.; Puchta, R.; Bugarčić, Ž.D.; Van Eldik, R. Studies on the Reactions of $[AuCl_4]^-$ with Different Nucleophiles in Aqueous Solution. *Dalton Trans.* **2014**, *43*, 8620–8632. [CrossRef]
20. Mironov, I.V.; Tsvelodub, L.D. Equilibria of Cl- substitution by pyridine, 2,2′-dipyridine, 1,10-phenantroline in $AuCl_4^-$ in aqueous solution. *Zhurn. Neorg. Khim.* **2001**, *46*, 154–159.
21. Mironov, I.V.; Tsvelodub, L.D. Equilibria of Cl- substitution by ammonia, ethylenediamine, diethylenetriamine in $AuCl_4^-$complex in aqueous solution. *Zhurn. Neorg. Khim.* **2000**, *45*, 425–430.

22. Mironov, I.V.; Kharlamova, V.Y.; Kokovkin, V.V. Application of Capillary Electrophoresis to the Study of Equilibria on an Example of Gold(III) Complexes. *J. Anal. Chem.* **2018**, *73*, 586–592. [CrossRef]
23. Mironov, I.V.; Kharlamova, V.Y.; Kokovkin, V.V. Investigation of Chloride Ion Substitution Equilibria in $AuCl_4^-$ with Ethylenediamine and 1,3-Diaminopropane Using Capillary Zone Electrophoresis. *Russ. J. Inorg. Chem.* **2018**, *63*, 134–139. [CrossRef]
24. Byriel, K.; Dunster, K.R.; Gahan, L.R.; Kennard, C.H.L.; Latten, J.L.; Swann, I.L.; Duckworth, P.A. Lead Macrocyclic Complexes: The Synthesis, Complex Formation and X-Ray Crystal Structures of [Pb(L1)(NO3)2] and [Pb(L2)(NO3)2] (L1 = 1,4,7,10-Tetraoxa-13-Azacyclopentadecane, L2 = 1,4,7,10,13-Pentaoxa-16-Azacyclooctadecane). *Polyhedron* **1992**, *11*, 1205–1212. [CrossRef]
25. Byriel, K.A.; Dunster, K.R.; Gahan, L.R.; Kennard, C.H.L.; Latten, J.L.; Swann, I.L.; Duckworth, P.A. Stability Constants of the Zinc(II), Cadmium(II) and Mercury(II) Complexes of the Mono-Aza Coronands 1,4,7,10-Tetraoxa-13-Azacyclopentadecane (L1), 1,4,7,10,13-Pentaoxa-16-Azacyclooctadecane (L2) and 1,4,7-Trioxa-10-Azacyclododecane (L3). Crystal and Molecular Structures of the Cadmium Complexes of L1 and L2. *Inorg. Chim. Acta* **1993**, *205*, 191–198. [CrossRef]
26. Kuranova, N.N.; Usacheva, T.R.; Gushschina, A.S.; Kryukova, O.V.; Belova, N.V.; Lan, P.T. Thermodynamic and Structural Parameters of Protolytic Equilibria of 1-Aza-18-crown-6 in Aqueous Ethanol and Aqueous Dimethyl Sulfoxide. *Ross. Khimicheskii Zhurnal* **2025**, *69*, 107–114. [CrossRef]
27. Isaeva, V.A.; Katolikova, A.S. Protonation Constants of Cryptand[2.2] in Aqueous Dimethyl Sulfoxide Solutions. *Russ. J. Phys. Chem.* **2025**, *99*, 1288–1294. [CrossRef]
28. Isaeva, V.A.; Sharnin, V.A. Effect of Water–Ethanol Solvents on the Protonation Constants of Cryptand[2.2.2]. *Russ. J. Phys. Chem.* **2018**, *92*, 710–713. [CrossRef]
29. Rowan Labs. Available online: https://labs.rowansci.com (accessed on 3 March 2026).
30. Wagen, C.; Wagen, A. Efficient and Accurate pKa Prediction Enabled by Pre-Trained Machine-Learned Interatomic Potentials. 2024, preprint. [CrossRef]
31. Gaikwad, A.G.; Noguchi, H.; Yoshio, M. Stability Constants of Crown Ether Complexes with Aqueous Hydronium Ion. *Anal. Sci.* **1987**, *3*, 217–220. [CrossRef]
32. Isaeva, V.A.; Katolikova, A.S.; Grazhdan, K.V. Stability of Copper(II) Complexes with Cryptand[2.2.2] in Aqueous Dimethyl Sulfoxide Solutions. *Russ. J. Phys. Chem.* **2025**, *99*, 1280–1287. [CrossRef]
33. Isaeva, V.A.; Katolikova, A.S.; Pogodina, E.I.; Kuranova, N.N. Effect of the Composition of a Water–Dimethyl Sulfoxide Solvent on the Stability of Nickel(II)–Cryptand[2.2.2] Complexes. *Russ. J. Phys. Chem.* **2024**, *98*, 1648–1655. [CrossRef]
34. Arenaza-Corona, A.; Morales-Morales, D.; Hernández-Ahuactzi, I.F.; Barba, V. Structural and Conformational Changes in [M(1,10-Diaza-18-Crown-6)Cl_2] (M = Pd, Pb) Complexes: A Crystallographic and Theoretical Study. *CrystEngComm* **2018**, *20*, 6733–6740. [CrossRef]
35. Shannon, R.D. Revised Effective Ionic Radii and Systematic Studies of Interatomic Distances in Halides and Chalcogenides. *Acta Cryst. A* **1976**, *32*, 751–767. [CrossRef]
36. Chernyshev, A.N.; Kukushkin, V.Y.; Haukka, M. Two Complexes of Pt^{IV} and Au^{III} with 2,2′-Dipyridylamine and 2,2′-Dipyridylaminide Ligands. *Acta Crystallogr. C Struct. Chem.* **2014**, *70*, 1133–1137. [CrossRef] [PubMed]
37. Mironov, I.V.; Tsvelodub, L.D. Chlorohydroxocomplexes of gold(III) in aqueous alkaline solutions. *Zhurn. Neorg. Khim.* **2000**, *45*, 706–711.
38. Mironov, I.V.; Makotchenko, E.V. The Hydrolysis of AuCl 4 − and the Stability of Aquachlorohydroxocomplexes of Gold(III) in Aqueous Solution. *J. Solut. Chem.* **2009**, *38*, 725–737. [CrossRef]
39. Mironov, I.V.; Kharlamova, V.Y. Gold(III) Chlorohydroxo Complexes in Aqueous Solutions at Increased Temperatures. *Russ. J. Inorg. Chem.* **2020**, *65*, 420–425. [CrossRef]
40. Skibsted, L.H.; Bjerrum, J.; Frederichsen, P.S.; Nakken, K.F. Studies on Gold Complexes. I. Robustness, Stability and Acid Dissociation of the Tetramminegold(III) Ion. *Acta Chem. Scand.* **1974**, *28a*, 740–746. [CrossRef]
41. Zavalishin, M.N.; Pimenov, O.A.; Belov, K.V.; Khodov, I.A.; Gamov, G.A. Chemical Equilibria in Aqueous Solutions of H[AuCl4] and Bovine or Human Serum Albumin. *J. Mol. Liq.* **2023**, *389*, 122914. [CrossRef]
42. Logacheva, O.I.; Pimenov, O.A.; Gamov, G.A. UV–Vis Spectra of Gold(III) Complexes with Different Halides, Hydroxide, and Ammonia According to TD-DFT Calculations. *Chemistry* **2025**, *8*, 3. [CrossRef]
43. Gamov, G.A.; Meshkov, A.N.; Zavalishin, M.N.; Petrova, M.V.; Khokhlova, A.Y.; Gashnikova, A.V.; Sharnin, V.A. Binding of Pyridoxal, Pyridoxal 5′-Phosphate and Derived Hydrazones to Bovine Serum Albumin in Aqueous Solution. *Spectrochim. Acta Part A Mol. Biomol. Spectrosc.* **2020**, *233*, 118165. [CrossRef]
44. Sabatini, A.; Sacconi, L.; Schettino, V. Far-Infrared Spectra and Vibrational Force Constants of the Ions $AuCl_4^-$, $AuBr_4^-$, and $PtCl_4^{2-}$. *Inorg. Chem.* **1964**, *3*, 1775–1776. [CrossRef]
45. Zhang, H.; Wang, X.; Wang, Y.; Zhang, Y.; Zhang, W.; You, W. Alkaline-Stable Anion-Exchange Membranes with Barium [2.2.2]Cryptate Cations: The Importance of High Binding Constants. *Angew. Chem. Int. Ed.* **2023**, *62*, e202217742. [CrossRef]

46. Brachvogel, R.-C.; Maid, H.; Von Delius, M. NMR Studies on Li+, Na+ and K+ Complexes of Orthoester Cryptand o-Me2-1.1.1. *IJMS* **2015**, *16*, 20641–20656. [CrossRef]
47. Mei, E.; Popov, A.I.; Dye, J.L. Cesium-133 Nuclear Magnetic Resonance Study of Complexation by Cryptand C222 in Various Solvents: Evidence for Exclusive and Inclusive Complexes. *J. Am. Chem. Soc.* **1977**, *99*, 6532–6536. [CrossRef]
48. Rich, R.L.; Taube, H. The Uncatalyzed Exchange of Cl^- and $AuCl_4^-$. *J. Phys. Chem.* **1954**, *58*, 1–5. [CrossRef]
49. Makotchenko, E.V.; Kharlamova, V.Y.; Baidina, I.A.; Bardina, E.E.; Korolkov, I.V.; Mironov, I.V.; Gushchin, A.L. Synthesis, Crystal Structure and Solution Studies of Gold(III) Complexes with 1,1-Dimethylbiguanide. *Inorg. Chim. Acta* **2023**, *552*, 121496. [CrossRef]
50. Al-Maythalony, B.A.; Wazeer, M.I.M.; Isab, A.A. 1H, 13C NMR and UV Spectroscopy Studies of Gold(III)-Tetracyanide Complex with l-Cysteine, Glutathione, Captopril, l-Methionine and Dl-Seleno-Methionine in Aqueous Solution. *Inorg. Chim. Acta* **2010**, *363*, 3244–3253. [CrossRef]
51. Brown, R.K.; Bunyan, J.N.; Agrawal, A.; Li, G.; Dautoras, D.; Sarker, J.C.; Keat, T.T.; Hicks, T.; Hogarth, G.; Pugh, D. A Revised Understanding of the Speciation of Gold(III) Dithiocarbamate Complexes in Solution. *Dalton Trans.* **2025**, *54*, 7627–7640. [CrossRef]
52. Radisavljević, S.; Petrović, B. Gold(III) Complexes: An Overview on Their Kinetics, Interactions With DNA/BSA, Cytotoxic Activity, and Computational Calculations. *Front. Chem.* **2020**, *8*, 379. [CrossRef]
53. Broennum, B.; Johansen, H.S.; Skibsted, L.H. Ammine Ligand Exchange in Tetraamminegold(III) in Aqueous Solution. Composition of Transition States and Relative Reactivity of Tetraamminegold(III) and Its Conjugated Base, Amidotriamminegold(III). *Inorg. Chem.* **1988**, *27*, 1859–1862. [CrossRef]
54. Baddley, W.H.; Basolo, F. A Kinetic Study of Substitution Reactions of Some Gold(III) Complexes. *Inorg. Chem.* **1964**, *3*, 1087–1091. [CrossRef]
55. Drougge, L.; Elding, L.I. Mechanism for Oxidation of Tetracyanoplatinate(II) by Gold(III) Complexes. *Inorg. Chem.* **1987**, *26*, 1073–1077. [CrossRef]
56. Mandal, C.; Nandi, U.S. Kinetic Studies on the Interaction of Gold(III) with Nucleic Acids. I. Native DNA-Au(III) System-Spectrophotometric Studies. *Proc. Indian Acad. Sci. (Chem. Sci.)* **1979**, *88*, 263–278. [CrossRef]
57. León, F.; García-Rodeja, Y.; Mallet-Ladeira, S.; Miqueu, K.; Szalóki, G.; Bourissou, D. Catechol/*o*-Benzoquinone Exchange at Gold(III). *Chem. Sci.* **2024**, *15*, 16651–16659. [CrossRef]
58. Vugrin, L.; Halasz, I.; Geneste, H. Characterization and Isolation of an 18-Crown-6 Complex of Potassium Hydroxide Prepared by Milling: Application to Mechanochemical Organic Synthesis. *New J. Chem.* **2023**, *47*, 7466–7469. [CrossRef]
59. Li, S.; Lin, L.; Wang, W.; Yan, X.; Chen, B.; Jiang, S.; Liu, S.; Ma, X.; Tian, H.; Yu, X. Aza-Crown Ether Locked on Polyethyleneimine: Solving the Contradiction between Transfection Efficiency and Safety during in Vivo Gene Delivery. *Chem. Commun.* **2020**, *56*, 5552–5555. [CrossRef] [PubMed]
60. Soo, K.C.; Yu, S.Y.; Jin, U.K.; Jeong, K.K. Manufacturing Method of Novel Ion Exchange Material. KR102009180B1, 21 October 2019.
61. You, D.; Li, K.; Chang, Y.; Wang, R.; He, R.; Zhou, L.; Li, M. Precise Modification of Organic Cations to Enhance the Moisture Stability and Luminescence Efficiency of Mn-Based Halides. *Inorg. Chem.* **2024**, *63*, 22935–22943. [CrossRef] [PubMed]
62. Pierre, J.L.; Handel, H.; Labbe, P.; Le Goaller, R. Positive Halogen Cryptate: Complexation of Iodine with [2.2.2] Cryptand. *J. Am. Chem. Soc.* **1980**, *102*, 6574–6575. [CrossRef]
63. Tsukube, H.; Takagi, K.; Higashiyama, T.; Iwachido, T.; Hayama, N. Specific Ag^+ Ion Binding and Transport Properties of 'Tripod' Type Open-Chain Cryptands. *J. Chem. Soc. Perkin Trans. 1* **1987**, 1697–1700. [CrossRef]
64. Babailov, S.P. Paramagnetic Properties and Molecular Structure of Coordination Saturated Inclusive Lanthanide Complexes with 18-Crown-6 Using NMR. *J. Incl. Phenom. Macrocycl. Chem.* **2014**, *80*, 377–381. [CrossRef]
65. Alizadeh, N.; Shamsipur, M. NMR Study of the Ligand Interchange of 18-Crown-6 Complexes with La^{3+}, Ca^{2+}, Pb^{2+} and Ba^{2+} Ions in 70% Methanol Solution. *Faraday Trans.* **1996**, *92*, 4391. [CrossRef]
66. Shamsipur, M.; Irandoust, M. A Proton NMR Study of the Stoichiometry and Stability of 18-Crown-6 Complexes with K^+, Rb^+ and Tl^+ Ions in Binary Dimethyl Sulfoxide-Nitrobenzene Mixtures. *J. Solut. Chem.* **2008**, *37*, 657–664. [CrossRef]
67. Gamov, G.A.; Yarullin, D.N.; Gudyrina, M.A.; Pogodina, E.I.; Medvedeva, A.S.; Zavalishin, M.N. Protonation of l-Ascorbic Acid in an Aqueous Solution at T = 298.2 K, p = 0.1 MPa, and I = 0.10–5.0 Mol L^{-1} (NaCl). *J. Chem. Eng. Data* **2022**, *67*, 1358–1364. [CrossRef]
68. Meshkov, A.N.; Gamov, G.A. KEV: A Free Software for Calculating the Equilibrium Composition and Determining the Equilibrium Constants Using UV–Vis and Potentiometric Data. *Talanta* **2019**, *198*, 200–205. [CrossRef]
69. Mironov, I.V.; Makotchenko, E.V. Equilibria in the System of Aquachlorohydroxogold(III) Complexes in Aqueous Solution. *Russ. J. Inorg. Chem.* **2009**, *54*, 2010–2017. [CrossRef]

70. Bandura, A.V.; Lvov, S.N. The Ionization Constant of Water over Wide Ranges of Temperature and Density. *J. Phys. Chem. Ref. Data* **2006**, *35*, 15–30. [CrossRef]
71. Liu, M.; Mao, X.; Ye, C.; Huang, H.; Nicholson, J.K.; Lindon, J.C. Improved WATERGATE Pulse Sequences for Solvent Suppression in NMR Spectroscopy. *J. Magn. Reson.* **1998**, *132*, 125–129. [CrossRef]

Disclaimer/Publisher's Note: The statements, opinions and data contained in all publications are solely those of the individual author(s) and contributor(s) and not of MDPI and/or the editor(s). MDPI and/or the editor(s) disclaim responsibility for any injury to people or property resulting from any ideas, methods, instructions or products referred to in the content.